

Gibbs Flow for Approximate Transport with Applications to Bayesian Computation

Jeremy Heng*, Arnaud Doucet* and Yvo Pokern†

February 24, 2021

*Department of Statistics, University of Oxford, UK.

†Department of Statistical Science, University College London, UK.

Abstract

Let π_0 and π_1 be two probability measures on \mathbb{R}^d , equipped with the Borel σ -algebra $\mathcal{B}(\mathbb{R}^d)$. Any measurable function $T : \mathbb{R}^d \rightarrow \mathbb{R}^d$ such that $Y = T(X) \sim \pi_1$ if $X \sim \pi_0$ is called a transport map from π_0 to π_1 . If for any π_0 and π_1 , one could obtain an analytical expression for a transport map from π_0 to π_1 then this could be straightforwardly applied to sample from any distribution. One would map draws from an easy-to-sample distribution π_0 to the target distribution π_1 using this transport map. Although it is usually impossible to obtain an explicit transport map for complex target distributions, we show here how to build a tractable approximation of a novel transport map. This is achieved by moving samples from π_0 using an ordinary differential equation whose drift is a function of the full conditional distributions of the target. Even when this ordinary differential equation is time-discretized and the full conditional distributions are approximated numerically, the resulting distribution of the mapped samples can be evaluated and used as a proposal within Markov chain Monte Carlo and sequential Monte Carlo schemes. We show experimentally that it can improve significantly performance of state-of-the-art sequential Monte Carlo methods for a fixed computational complexity.

Keywords: Mass transport; Markov chain Monte Carlo; Normalizing constants; Path Sampling; Sequential Monte Carlo.

1 Introduction

The use of the Bayesian formalism of inference is ubiquitous in many areas of science. For statistical models of practical interest, implementation usually relies on Monte Carlo methods to sample from the posterior distribution which might be high dimensional and exhibit complex dependencies. Most available Monte Carlo algorithms rely on proposal distributions and the efficiency of these techniques is crucially dependent on whether these proposals are able to capture the important features of the target. In this paper, we leverage ideas from the mass transport literature to develop a new methodology to build efficient proposal distributions which can be used within Markov chain Monte Carlo (MCMC) and sequential Monte Carlo (SMC).

Given two probability measures π_0, π_1 defined on $(\mathbb{R}^d, \mathcal{B}(\mathbb{R}^d))$, which in a Bayesian context may be interpreted as the prior and posterior, a transport map is a measurable function $T : \mathbb{R}^d \rightarrow \mathbb{R}^d$ such that $Y = T(X) \sim \pi_1$ if $X \sim \pi_0$. The transport map terminology arises from the fact that one can think of T as transporting the mass represented by π_0 to the mass represented by π_1 . We will use the standard notation $\pi_1 = T_{\#}\pi_0$ since π_1 is the push-forward measure of π_0 by T .

The existence and characterization of transport maps have generated a very large literature in mathematics; see [40] for a recent review. In particular, there has been much work dedicated to the L^2 Monge-Kantorovich problem where properties of the map T minimizing the expected cost $\mathbb{E}|Y - X|^2$ under the constraints $X \sim \pi_0$ and $Y \sim \pi_1$ have been analyzed.

In a Monte Carlo context, the availability of any analytically tractable transport map would allow us to map samples from π_0 to π_1 . Unfortunately, even without requiring the transport map to satisfy any optimality condition, such transport maps have only been identified in simple scenarios; e.g. when both π_0 and π_1 are Gaussian; e.g. [34]. To address this problem, [19] propose to minimize $\mathbb{E}_{X_0 \sim \pi_0} |Y - X|^2$ plus a term measuring the discrepancy between the distribution of $Y = \hat{T}_\beta(X)$ and π_1 over a set of maps parametrized by a finite-dimensional parameter β , e.g. a linear combination of some basis functions, to obtain an approximate transport map. Earlier work in statistics include [27] where a set of maps similarly parameterized by a finite-dimensional parameter is introduced and a discrepancy measure between π_0 and π_1 minimized w.r.t. to this parameter. However, it can be difficult to identify an appropriate subspace of candidate maps and the resulting optimization problems can be non-convex. In this paper, we follow a different approach where we directly exploit the structure of a novel transport map to build an approximate transport map. The methodology presented here neither requires selecting a parametric class of maps nor solving an optimization problem.

The transport map we approximate arises from a fluid dynamics interpretation of mass transport. Consider a curve of probability measures $\{\pi_t\}_{t \in (0,1)}$ allowing us to bridge π_0 to π_1 ; e.g. $\pi_t \propto \pi_0^{1-\lambda(t)} \pi_1^{\lambda(t)}$ where $\lambda : [0, 1] \rightarrow [0, 1]$ is a strictly increasing smooth function such that $\lambda(0) = 0$ and $\lambda(1) = 1$. This bridging idea is at the core of some of the most powerful Monte Carlo methods currently available such as path sampling [21] and Annealed Importance Sampling (AIS) [11, 24, 30]. If we perceive probability mass as an infinite ensemble of fluid particles, we could now attempt to prescribe an appropriate drift, called velocity field in this context, of an ordinary differential equation (ODE) to move these particles deterministically so as to mimic the time evolution of π_t over the pseudo-time interval $t \in [0, 1]$. Loosely speaking we may think of the action of particles under such a velocity field as implicitly defining the flow transport maps $\{T_t\}$ satisfying $\pi_t = T_{t\#}\pi_0$ for each $t \in [0, 1]$. The idea of building a transport map between π_0 and π_1 via a flow originates from [29]; see also [12, 22] for other early contributions. This approach has been recently adopted in a variety of areas ranging from electrical engineering to physics [4, 10, 14, 36, 38]. Noting that, for a given curve of measures, there could be multiple velocity fields defining flow transport maps verifying $\pi_t = T_{t\#}\pi_0$, various optimality criteria have been introduced to identify a unique solution [29, 32, 36]; e.g. [32] proposed selecting the velocity field minimizing kinetic energy. In these contributions, the optimal velocity field is given by the solution of an elliptic partial differential equation (PDE). However, when using a full grid, PDE solvers suffer from the the curse of dimensionality [13, 31] which renders them impractical. Sparse grid methods may be capable of dealing with sufficiently high dimensions but they come with their own set of approximations, e.g. tensor approximations [9, 13].

An alternative approach involves developing analytically tractable approximations of intractable flow transport maps. For example, in a Bayesian context where the prior π_0 on the unknown parameter X is a Gaussian distribution and the likelihood is Gaussian of mean $\phi(X)$ and constant variance, [7] proposed to linearize the likelihood locally to exploit the fact that we would have access to analytically tractable flow transport maps if the distributions $\{\pi_t\}$ were Gaussian; see e.g. [5, 33]. The resulting distribution of the samples of π_0 mapped by the approximate transport map is then used as an importance sampling distribution within a SMC scheme. The authors demonstrate very good performance in highly nonlinear filtering problems up to $d = 6$. Here we also propose analytically tractable approximate flow transport maps but the details of our construction are markedly different. Our approach does not require any distributional assumptions about π_0 and π_1 , instead it relies on the approximation of novel flow transport maps which can be thought of a flow version of the Knothe-Rosenblatt transport; see e.g. [40, p. 20]. If we write $\pi_t(dx) = \pi_t^{X_1, \dots, X_d}(dx_1, \dots, dx_d)$ then, as with the original Knothe-Rosenblatt transport, the resulting flow transport maps are typically intractable as they require analytical knowledge of the conditional distributions $\{\pi_t^{X_i | X_1, \dots, X_{i-1}}(dx_i | x_1, \dots, x_{i-1})\}_{i=2}^d$. We propose a tractable

approximation which moves particles using a velocity field designed to track the full conditional distributions $\{\pi_t^{X_i|X_{-i}}(dx_i|x_{-i})\}_{i=1}^d$, where $x_{-i} = (x_1, \dots, x_{i-1}, x_{i+1}, \dots, x_d)$, which we will refer to as the Gibbs flow in reference to the Gibbs sampler. To simplify notation, we will write abusively $\pi_t(dx_i|x_1, \dots, x_{i-1})$ and $\pi_t(dx_i|x_{-i})$ for the conditional distributions and full conditional distributions respectively. Similarly, we write $\pi_t(dx_i)$ for the marginal of X_i under π_t and will denote distributions and their associated densities w.r.t. to Lebesgue measure by the same symbol. Various properties of the Gibbs flow are established and we demonstrate experimentally its performance on a variety of statistical models in scenarios up to $d = 128$.

The rest of the paper is organized as follows. In Section 2, we review the flow formulation of the transport problem in a Bayesian context. In Section 3, we present a novel flow transport, its Gibbs flow approximation and properties of these flows. In Section 4, we show how the Gibbs flow can be used to build valid proposal distributions even when the ODE is time-discretized and full conditional distributions are approximated. Finally, we demonstrate the performance of the proposed methodology on a multimodal mixture model, truncated Gaussian distributions and a multivariate probit model in Section 5. All the proofs are given in the appendices.

2 Transport with flows

2.1 A curve from prior to posterior

Let $\pi_0(dx)$ be a prior probability measure on $(\mathbb{R}^d, \mathcal{B}(\mathbb{R}^d))$ and $L : \mathbb{R}^d \rightarrow \mathbb{R}^+$ denote a likelihood function. To simplify presentation, we shall assume that $\pi_0(dx)$ is absolutely continuous with respect to Lebesgue measure on \mathbb{R}^d , with an everywhere positive density $\pi_0(x)$ and that L is also positive everywhere¹. Notationally we will suppress all dependencies on observations. From Bayes' rule, the resulting target posterior $\pi(dx)$ admits the density

$$\pi(x) = \frac{\pi_0(x)L(x)}{Z}, \quad (1)$$

where $Z = \int_{\mathbb{R}^d} \pi_0(u)L(u) du$ denotes the marginal likelihood which we assume to be finite. Henceforth we shall additionally assume that $\pi_0, L \in C^1(\mathbb{R}^d, \mathbb{R}^+)$, where $C^k(A, B)$ denotes the set of functions from A to B which are k -times continuously differentiable.

We introduce a curve of measures $\mathcal{C}_\pi = \{\pi_t\}_{t \in [0,1]}$ smoothly bridging the prior π_0 to the posterior $\pi_1 = \pi$ by gradually introducing the likelihood using a strictly increasing C^1 -function $\lambda : [0, 1] \rightarrow [0, 1]$ such that $\lambda(0) = 0$ and $\lambda(1) = 1$:

$$\pi_t(x) = \frac{\pi_0(x)L(x)^{\lambda(t)}}{Z(t)}, \quad (2)$$

where $Z(t) = \int_{\mathbb{R}^d} \pi_0(u)L(u)^{\lambda(t)} du$. By differentiating (2) w.r.t. the pseudo-time variable t , we obtain

$$\partial_t \pi_t(x) = \lambda'(t) (\log L(x) - I_t) \pi_t(x), \quad (3)$$

where

$$I_t = \frac{1}{\lambda'(t)} \frac{d}{dt} \log Z(t) = \frac{\frac{d}{dt} \int_{\mathbb{R}^d} \pi_0(u)L(u)^{\lambda(t)} du}{\lambda'(t)Z(t)} = \mathbb{E}_{\pi_t}[\log L(X_t)] \quad (4)$$

is assumed finite. The last equality in (4) holds when the order of differentiation with respect to the pseudo-time variable and integration with respect to the state variable can be interchanged. From a statistical perspective, this assumes that the family of models $\{\pi_t\}_{t \in [0,1]}$ is regular so that

¹In Section 5.2, we deal with a specific case where the likelihood is allowed to be zero on a set of positive Lebesgue measure.

(4) is simply a consequence of the fact that the expectation of the score function is zero for each $t \in [0, 1]$. By integrating (4), we recover the well-known path sampling identity [21]:

$$\log Z = \int_0^1 \lambda'(t) I_t dt. \quad (5)$$

Equation (3) reveals that the expected log-likelihood I_t plays the role of a reference value which controls the evolution of the density $\pi_t(x)$, i.e. in logarithmic scale, the local behaviour around a point $x \in \mathbb{R}^d$ is such that there is an increase or decrease in density if $\log L(x) > I_t$ or $\log L(x) < I_t$ respectively. In what follows, we will see that this difference, when integrated w.r.t. $\pi_t(x)$, provides us with the right direction to move particles at time t . The factors $\pi_t(x)$ and $\lambda'(t)$ in (3) are also intuitive as the change in density must be proportional to how much probability mass there is locally and how quickly we introduce the likelihood. It will be apparent later that these factors dictate the speed of particles.

2.2 Particle dynamics and Liouville's equation

Consider a particle in \mathbb{R}^d initialized at time $t = 0$ with a random draw $X_0 \sim \pi_0$ and evolved deterministically according to the following ordinary differential equation (ODE)

$$\frac{dx}{dt} = f(x, t), \quad (6)$$

where $f : \mathbb{R}^d \times [0, 1] \rightarrow \mathbb{R}^d$ can be interpreted as a velocity field. Under appropriate regularity conditions on f which will be detailed later, this ODE admits a unique solution $x(t; X_0)$ for $t \in [0, 1]$ so the map $X_t = T_t(X_0) = x(t; X_0)$ is well defined and is a C^1 -diffeomorphism for each $t \in [0, 1]$. Additionally, if we denote as $\tilde{\pi}_t$ the law of X_t , the curve of distributions $\mathcal{C}_{\tilde{\pi}} = \{\tilde{\pi}_t\}_{t \in [0, 1]}$ satisfies, under regularity conditions, the Liouville PDE [20, eq. (3.5.13), p. 54] also known as the continuity equation [2, eq. (8.1.1), p. 169]:

$$\partial_t \tilde{\pi}_t(x) = - \sum_{i=1}^d \partial_{x_i} (\tilde{\pi}_t(x) f_i(x, t)), \quad (7)$$

where ∂_t and ∂_{x_i} denotes the partial derivative w.r.t. t and x_i respectively. We will write (7) more succinctly as

$$\partial_t \tilde{\pi}_t = -\nabla \cdot (\tilde{\pi}_t f). \quad (8)$$

An informal but intuitive derivation of Liouville's PDE is given in Appendix A. We will call $\mathcal{C}_{\tilde{\pi}} = \{\tilde{\pi}_t\}_{t \in [0, 1]}$ a weak solution of (8) if

$$\int_0^1 \int_{\mathbb{R}^d} (\partial_t \varphi + \langle f, \nabla \varphi \rangle) \tilde{\pi}_t(x) dx dt = 0 \quad (9)$$

for all compactly supported $\varphi \in C^\infty(\mathbb{R}^d \times [0, 1], \mathbb{R})$ where $\langle \cdot, \cdot \rangle$ denotes the scalar product in \mathbb{R}^d , $|\cdot|$ the Euclidean norm and $\nabla \varphi = (\partial_{x_1} \varphi, \dots, \partial_{x_d} \varphi)^T$.

2.3 Flow transport problem and regularity conditions

Given the curve of target measures \mathcal{C}_π in (2) and Liouville's PDE (8), the flow transport problem involves identifying a velocity field such that $\mathcal{C}_\pi = \{\pi_t\}_{t \in [0, 1]}$ is a weak solution of Liouville equation (8). However, this velocity field should also be regular enough that the resulting ODE (6) admits a unique solution globally defined on $[0, 1]$. We discuss here sufficient regularity conditions ensuring equivalence between the PDE solution, commonly referred to as the Eulerian approach, and the ODE solution, which is typically called the Lagrangian approach.

Definition 1. Let $\mathcal{L}(\mathcal{C}_\pi)$ denote the set of all velocity fields such that $\mathcal{C}_\pi = \{\pi_t\}_{t \in [0,1]}$ is a weak solution of the Liouville equation (8) on $\mathbb{R}^d \times (0, 1)$.

Definition 2. Let $\mathcal{E}(\mathcal{C}_\pi)$ be the set of all velocity fields satisfying the following conditions:

- **A1.** (local Lipschitz continuity) f is a Borel function and is locally Lipschitz in the spatial variable, i.e. for every compact set $K \subset \mathbb{R}^d$, there exists $M(K) > 0$ such that $|f(x, t) - f(y, t)| \leq M(K)|x - y|$ for all $(x, t), (y, t) \in K \times [0, 1]$;
- **A2.** (space-time integrability) $\int_0^1 \int_{\mathbb{R}^d} |f(x, t)| \pi_t(x) \, dx dt < \infty$.

We first establish a preliminary result before giving the main theorem.

Lemma 1. *The curve of measures $\mathcal{C}_\pi = \{\pi_t\}_{t \in [0,1]}$ defined in (2) is narrowly continuous, i.e. for any bounded function $\varphi \in C^0(\mathbb{R}^d, \mathbb{R})$ and any sequence $(t_n)_{n \geq 1} \subset [0, 1]$ such that $t_n \rightarrow t_*$ we have*

$$\lim_{n \rightarrow \infty} \int_{\mathbb{R}^d} \varphi(x) \pi_{t_n}(dx) = \int_{\mathbb{R}^d} \varphi(x) \pi_{t_*}(dx).$$

Theorem 1. ([2, Lemma 8.1.6, Proposition 8.1.8]) *Let f be a velocity field in $\mathcal{L}(\mathcal{C}_\pi) \cap \mathcal{E}(\mathcal{C}_\pi)$, then the following two statements are equivalent:*

(Eulerian perspective) the narrowly continuous curve $\mathcal{C}_\pi = \{\pi_t\}_{t \in [0,1]}$ is a weak solution of Liouville equation (8) on $\mathbb{R}^d \times (0, 1)$;

(Lagrangian perspective) for π_0 -almost all $x_0 \in \mathbb{R}^d$, there exists a unique solution $x(t; x_0)$ to the ODE (6) globally defined on $[0, 1]$, therefore the flow maps $T_t(x_0) = x(t; x_0)$ are well defined and satisfy the flow transport property, i.e. $\pi_t = T_{t\#} \pi_0$ for each $t \in [0, 1]$.

Condition A1 is an assumption which provides existence of a unique solution to (6) on a unique maximal time interval $i(x_0)$ for each initial condition $x_0 \in \mathbb{R}^d$ [2, Lemma 8.1.4, p. 172]; we note that it only requires f to be a Borel function whereas standard results require $f \in C^0(\mathbb{R}^d \times [0, 1], \mathbb{R}^d)$ [41, Theorem III.3.VII, p. 108]. However, this time interval $i(x_0)$ may not contain $[0, 1]$, hence condition A2 acts as a supplementary condition to ensure that $i(x_0) = [0, 1]$. It is possible to weaken condition A1; see [1], [2, Theorem 8.2.1] for recent advances and [17] for earlier work. We note that condition A2 in particular implies

$$|f(x, t)| \pi_t(x) \rightarrow 0 \text{ as } |x| \rightarrow \infty. \quad (10)$$

We shall refer to velocity fields that satisfy (10) as having the vanishing property. We emphasize that these regularity conditions are not mere mathematical subtleties one can ignore. This will be illustrated in the next Section where we exhibit a velocity field in $\mathcal{L}(\mathcal{C}_\pi)$ which provably provides divergent particle trajectories.

Hence, formally, the flow transport problem involves identifying a velocity field in $\mathcal{L}(\mathcal{C}_\pi) \cap \mathcal{E}(\mathcal{C}_\pi)$. We will show in Proposition 2 that this set is non-empty and, as alluded to in the Introduction, this problem is typically underdetermined as illustrated in the following example.

Example 1. Consider $\pi_t = \mathcal{N}((0, 0)^T, I_2)$ for $t \in [0, 1]$ where $\mathcal{N}(\mu, \Sigma)$ denotes a Gaussian distribution of mean μ and covariance Σ and I_d the $d \times d$ identity matrix. The two time-invariant velocity fields $f_1(x_1, x_2) = (0, 0)^T$ and $f_2(x_1, x_2) = (-x_2, x_1)$ both lie in $\mathcal{L}(\mathcal{C}_\pi) \cap \mathcal{E}(\mathcal{C}_\pi)$.

Various optimality criteria have been employed to attain unicity but lead to elliptic PDEs. We ignore such criteria and instead concentrate on exhibiting a solution to the flow transport problem which is not represented as the solution of a PDE.

3 A novel flow transport and Gibbs flow approximation

3.1 A flow transport solution on \mathbb{R}

We first discuss the one-dimensional case $d = 1$ as our novel flow transport for $d > 1$ partially builds upon it. In this case, there is a rather well-known solution to the flow transport problem; see e.g. [4]. We establish here that this coincides with the minimal kinetic energy solution adopted by [32, 33].

Proposition 1. *Define the velocity field $f : \mathbb{R} \times [0, 1] \rightarrow \mathbb{R}$ as*

$$f(x, t) = \frac{-\int_{-\infty}^x \partial_t \pi_t(u) du}{\pi_t(x)}. \quad (11)$$

If there exists an $\epsilon > 0$ such that $x \mapsto |f(x, t)| \pi_t(x) = O(|x|^{-1-\epsilon})$ as $|x| \rightarrow \infty$ with a constant that is independent of $t \in [0, 1]$, then the velocity field (11) lies in $\mathcal{L}(\mathcal{C}_\pi) \cap \mathcal{E}(\mathcal{C}_\pi)$ and thus solves the flow transport problem on \mathbb{R} . It is additionally the minimal kinetic energy solution, i.e. for each $t \in [0, 1]$

$$f(\cdot, t) = \operatorname{argmin}_{g \in L^2(\pi_t) \cap \mathcal{L}(\pi_t)} \frac{1}{2} \int_{\mathbb{R}^d} g^2(x) \pi_t(x) dx, \quad (12)$$

where $L^2(\pi_t) = \{\varphi : \mathbb{R}^d \rightarrow \mathbb{R} : \int_{\mathbb{R}^d} \varphi^2(x) \pi_t(dx) < \infty\}$ and $\mathcal{L}(\pi_t)$ denotes the set of all classical solutions to Liouville equation at $t \in [0, 1]$, i.e. satisfying (8) at $t \in [0, 1]$ given $\mathcal{C}_{\bar{\pi}} = \mathcal{C}_\pi$.

We note that the velocity field (11) satisfies the vanishing property by construction as $x \mapsto \int_{-\infty}^x \partial_t \pi_t(u) du$ vanishes in the tails. From (3), (11) may be rewritten as

$$f(x, t) = \frac{\lambda'(t) I_t (F_t(x) - I_t^x / I_t)}{\pi_t(x)}, \quad (13)$$

where $I_t^x = \int_{-\infty}^x \log L(u) \pi_t(u) du$ and $F_t(x) = \int_{-\infty}^x \pi_t(u) du$ is the Cumulative Distribution Function (CDF) of π_t . In the Lagrangian perspective, the flow transport (13) may be likened to driving a vehicle. The denominator corresponds to the accelerator, since, for example, particles in the tails of π_t need to speed up to meet the changing schedule of intermediate distributions. Also, it is intuitive that particle speeds are proportional to the rate $\lambda'(t)$ at which we introduce the likelihood. The numerator amounts to the steering wheel: a particle's direction of travel is given by the relative difference between its current location x , described by the term $F_t(x)$, and where the particle needs to go, prescribed by the term $I_t^x / I_t \in [0, 1]$ which contains information from the likelihood. We investigate the behavior of this flow in a Gaussian scenario.

Example 2. Consider $\pi_0 = \mathcal{N}(\mu_0, \Sigma_0)$ and a likelihood $L(x) = \exp(-\frac{1}{2}(x - y)^T \Sigma_L^{-1}(x - y))$ corresponding to an observation $y \in \mathbb{R}^d$. Hence we have $\pi_t = \mathcal{N}(\mu_t, \Sigma_t)$ where

$$\mu_t = (\Sigma_0^{-1} + \lambda(t) \Sigma_L^{-1})^{-1} (\Sigma_0^{-1} \mu_0 + \lambda(t) \Sigma_L^{-1} y), \quad \Sigma_t^{-1} = \Sigma_0^{-1} + \lambda(t) \Sigma_L^{-1}, \quad (14)$$

and

$$I_t = -\frac{1}{2} (\operatorname{tr}(\Sigma_L^{-1} \Sigma_t) + (\mu_t - y)^T \Sigma_L^{-1} (\mu_t - y)). \quad (15)$$

In this Gaussian setting, the elliptic PDE providing the velocity field with minimum kinetic energy $\frac{1}{2} \int_{\mathbb{R}^d} f(x, t)^T \Sigma_t^{-1} f(x, t) \pi_t(x) dx$ can be solved analytically and its solution is (as given in [5]):

$$f_{\text{KE}}(x, t) = -\frac{\lambda'(t)}{2} \Sigma_t \Sigma_L^{-1} (\mu_t - 2y + x). \quad (16)$$

As noted in Proposition 1, the solution in (11) corresponds exactly to (16) in the $d = 1$ case. As a more concrete example to build intuition, we shall consider the case when $d = 1, \mu_0 = 0, \Sigma_0 =$

$1, y = 0, \Sigma_L = 1$. Now the curve is given by $\pi_t = \mathcal{N}\left(0, \frac{1}{1+\lambda(t)}\right)$, so as time progresses, we expect particles to have a mean-reverting behaviour towards the origin. Indeed, this is the case with the linear mean-reverting drift of $f(x, t) = -\frac{\lambda'(t)x}{2(\lambda(t)+1)}$ in (13). Figure 1 also illustrates this with the steering property mentioned earlier: since $I_t = -\frac{1}{2(1+\lambda(t))} < 0$ for all $t \in [0, 1]$, reversion to the stable stationarity point at the origin dictates that $F_t(x) < I_t^x/I_t$ for $x < 0$ and $F_t(x) > I_t^x/I_t$ for $x > 0$.

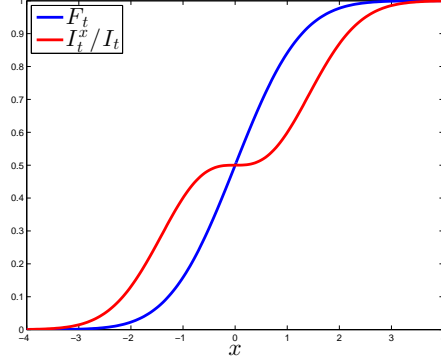


Figure 1: Illustrating steering property of (13) on univariate Gaussian example with $\lambda(t) = t$ and $t = 0$.

3.2 An incorrect flow transport on \mathbb{R}^d , $d \geq 2$

It is tempting to extend the flow transport solution of Proposition 1 from \mathbb{R} to \mathbb{R}^d , $d \geq 2$, by simply introducing the velocity field $\bar{f} = (\bar{f}_1, \dots, \bar{f}_d)$ given for $i = 1, 2, \dots, d$ by

$$\bar{f}_i(x, t) = \frac{-\gamma_i \int_{-\infty}^{x_i} \partial_t \pi_t(u_i, x_{-i}) du_i}{\pi_t(x)}, \quad (17)$$

where $\gamma_i \in \mathbb{R}$ and the integrand of (17) is to be understood as $\partial_t \pi_t(x_1, \dots, x_{i-1}, u_i, x_{i+1}, \dots, x_d)$. This velocity field has been previously mentioned in [4] and it can easily be shown that $\bar{f} \in \mathcal{L}(\mathcal{C}_\pi)$ whenever $\sum_{i=1}^d \gamma_i = 1$. However it is clear that $\pi_t(x) |\bar{f}_i(x, t)| \rightarrow 0$ as $x_i \rightarrow \infty$ for any $i = 1, 2, \dots, d$, so condition A2 does not hold. Hence $\bar{f} \notin \mathcal{E}(\mathcal{C}_\pi)$ so Theorem 1 does not apply. On a simple Gaussian example detailed below, we show that this velocity field results in diverging trajectories of the ODE (6).

Example 3. Consider $\pi_t = \mathcal{N}(\mu_t, \Sigma_t)$ with parameters given by (14) where $\mu_0 = (0, 0)^T$, $\Sigma_0 = \Sigma_L = I_2$ and $y = (0, 0)^T$. This setup corresponds to considering independent components marginally distributed according to the univariate Gaussian model of Example 2. Hence we would expect a particle following the ODE (6) to have a mean-reverting behaviour towards the origin. The velocity field in (17) is given by

$$\begin{pmatrix} \bar{f}_1(x, t) \\ \bar{f}_2(x, t) \end{pmatrix} = \begin{pmatrix} \frac{\gamma_1 \lambda'(t)}{2\pi_t(x_1)} \left(\int_{-\infty}^{x_1} u_1^2 \pi_t(u_1) du_1 + x_2^2 F_t(x_1) - \frac{F_t(x_1)}{1+\lambda(t)} \right) \\ \frac{\gamma_2 \lambda'(t)}{2\pi_t(x_2)} \left(\int_{-\infty}^{x_2} u_2^2 \pi_t(u_2) du_2 + x_1^2 F_t(x_2) - \frac{F_t(x_2)}{1+\lambda(t)} \right) \end{pmatrix} \quad (18)$$

for $x = (x_1, x_2)^T \in \mathbb{R}^2$ and $t \in [0, 1]$, where $\pi_t = \mathcal{N}\left((0, 0)^T, \frac{I_2}{1+\lambda(t)}\right)$ and $F_t(x_i)$ denotes the marginal CDFs. We note that the two components of the velocity field are coupled.

Now consider $\gamma_1, \gamma_2 > 0$ with $\gamma_1 + \gamma_2 = 1$. We investigate the behavior of particles in the upper-right quadrant of the space. For each $t \in [0, 1]$, define the sets $\mathcal{S}_t = \left\{x \in \mathbb{R}^2 : x_1, x_2 > 1/\sqrt{1+\lambda(t)}\right\}$ and $\mathcal{P}_t = \{x \in \mathbb{R}^2 : \bar{f}(x, t) > (0, 0)^T\}$; noting that $\lambda'(t) > 0$, it follows from (18) that $\mathcal{S}_0 \subset \mathcal{S}_t \subset \mathcal{P}_t$

for any $t \in (0, 1]$. Since $\pi_0(\mathcal{S}_0) > 0$, we can conclude that there exist particle trajectories which only move farther away from the origin with positive probability. Analytical tractability in this simple example allows us to strengthen the previous statement and show that these trajectories in fact blow up in finite time. We start by seeking a lower bound on \bar{f} ; by symmetry, it suffices to consider only the first component. On the set \mathcal{S}_0 we have $\int_{-\infty}^{x_1} u_1^2 \pi_t(u_1) du_1 > \frac{1}{2(1+\lambda(t))} \geq \frac{1}{4}$, hence

$$\bar{f}_1(x, t) \geq \frac{c}{4} \exp\left(\frac{1}{2}x_1^2\right) \geq \frac{c}{32}x_1^4, \quad (19)$$

where $c = \frac{\gamma_1 \sqrt{\pi}}{2} \inf_{t \in [0, 1]} \lambda'(t) > 0$. Now define the uncoupled system

$$\begin{pmatrix} \hat{f}_1(x_1, t) \\ \hat{f}_2(x_2, t) \end{pmatrix} = \begin{pmatrix} \frac{c}{32}x_1^4 \\ \frac{c}{32}x_2^4 \end{pmatrix} \leq \begin{pmatrix} \bar{f}_1(x, t) \\ \bar{f}_2(x, t) \end{pmatrix}, \quad (20)$$

and note that its solution $x_i(t; x_{0,i}) = 1/\sqrt[3]{3\left(\frac{1}{3cx_{0,i}^3} - \frac{c}{32}t\right)}$, corresponding to the initial condition $x_0 = (x_{0,1}, x_{0,2})^T \in \mathbb{R}^2$, diverges as $t \rightarrow \frac{32}{3cx_{0,i}^3}$. Define the set $\mathcal{V} = \left\{x \in \mathbb{R}^2 : x_1, x_2 > \sqrt[3]{\frac{32}{3c}}\right\}$. Noting that \hat{f} is locally Lipschitz and component-wise increasing, the comparison theorem [41, Theorem III.10.XII (b), p. 112] implies that a particle starting in $\mathcal{S}_0 \cap \mathcal{V}$ and evolving under (18) has a trajectory that explodes before $t = 1$. Since $\pi_0(\mathcal{S}_0 \cap \mathcal{V}) > 0$, we conclude the claim that there exist divergent particle trajectories with positive probability.

3.3 A novel flow transport on \mathbb{R}^d , $d \geq 1$

The main reason why the flow induced by the velocity field \bar{f} in (17) does not solve the flow transport problem for $d \geq 2$ is that \bar{f} does not vanish in the tails. We show here how the introduction of some regularizing functions allows us to resolve this issue. For notational simplicity, write $x_{i:j}$ for the vector $(x_i, \dots, x_j)^T \in \mathbb{R}^{j-1+1}$.

Proposition 2. *Let $g_i \in C^2(\mathbb{R}, [0, 1])$, for $i = 1, 2, \dots, d-1$, be non-decreasing functions with the following tail behavior: $g_i(x_i, t) \rightarrow 0$ as $x_i \rightarrow -\infty$ and $g_i(x_i, t) \rightarrow 1$ as $x_i \rightarrow \infty$. Denote partial derivatives $\partial_{x_i} g_i(x_i, t)$ by $g'_i(x_i, t)$ and define the velocity field $f : \mathbb{R}^d \times [0, 1] \rightarrow \mathbb{R}^d$ as*

$$\begin{aligned} f_i(x, t) = & - \left(\prod_{j=1}^{i-1} g'_j(x_j, t) \int_{-\infty}^{x_i} \int_{\mathbb{R}^{i-1}} \partial_t \pi_t(u_{1:i-1}, u_i, x_{i+1:d}) du_{1:i-1} du_i \right. \\ & \left. - \prod_{j=1}^{i-1} g'_j(x_j, t) g_i(x_i, t) \int_{\mathbb{R}^i} \partial_t \pi_t(u_{1:i}, x_{i+1:d}) du_{1:i} \right) / \pi_t(x) \end{aligned} \quad (21)$$

for $i = 1, 2, \dots, d-1$ (use the convention $\prod_1^0 := 1$) and

$$f_d(x, t) = - \left(\prod_{j=1}^{d-1} g'_j(x_j, t) \int_{-\infty}^{x_d} \int_{\mathbb{R}^{d-1}} \partial_t \pi_t(u_{1:d-1}, u_d) du_{1:d-1} du_d \right) / \pi_t(x). \quad (22)$$

If there exists an $\epsilon > 0$ such that $x \mapsto |f(x, t)| \pi_t(x) = O(|x|^{-1-\epsilon})$ as $|x| \rightarrow \infty$ with a constant that is independent of $t \in [0, 1]$, then the velocity field (21)-(22) lies in $\mathcal{L}(\mathcal{C}_\pi) \cap \mathcal{E}(\mathcal{C}_\pi)$ and thus solves the flow transport problem on \mathbb{R}^d .

As before, we note that $|f| \pi_t$ satisfies the vanishing property by construction. Indeed $|f_i| \pi_t$ vanishes in the tails for $i = 1, 2, \dots, d-1$ as this is so of $\partial_t \pi_t$ and our assumptions imply that $g'_i(x_i, t) \rightarrow 0$ as $|x_i| \rightarrow \infty$. This also holds for $|f_d| \pi_t$, using, additionally, the fact that $\int_{\mathbb{R}^d} \partial_t \pi_t(u) du = 0$.

Note that Proposition 2 recovers Proposition 1 in the $d = 1$ case. A careful inspection of (21)-(22) reveals that the dynamics are constructed to track changes in the underlying conditionals

$\{\pi_t(dx_i|x_1, \dots, x_{i-1})\}_{i=2}^d$ and in this sense may be thought of as the flow transport analogue of the well-known Knothe-Rosenblatt transport [40, p. 20]. This flow transport is a generalization of the approach proposed by [6] in a molecular quantum chemistry context to build a compactly supported three-dimensional velocity field solving the flow transport problem.

Proposition 2 leaves a degree of freedom over the choice of scalar functions $\{g_i\}_{i=1}^{d-1}$. We advocate that it is a sensible choice to select $\{g_i\}_{i=1}^{d-1}$ such that the vector field on \mathbb{R}^d reduces to d many independent vector fields on \mathbb{R} if the target factorizes, that is if $\pi_t(x) = \prod_{i=1}^d \pi_t(x_i)$ where $\pi_t(x_i) = \pi_0(x_i)L_i(x_i)^{\lambda(t)}/Z_i(t)$. More precisely, we would like the original Liouville equation defined on $\mathbb{R}^d \times (0, 1)$ to simplify to a system of uncoupled Liouville PDEs each defined on $\mathbb{R} \times (0, 1)$:

$$-\partial_{x_i}(\pi_t(x_i)f_i(x_i, t)) = \partial_t \pi_t(x_i) \quad \text{for } i = 1, 2, \dots, d, \quad (23)$$

and solved by Proposition 1. We shall refer to velocity fields which exhibit this behaviour as having the factorization under independence property.

Proposition 3. *If $g_i(x_i, t) = F_t(x_i)$ for $i = 1, 2, \dots, d - 1$, then the velocity field defined in (21)-(22) factorizes if the posterior factorizes.*

The above result is intuitive: although the validity of Proposition 2 holds for any suitable scalar functions $\{g_i\}_{i=1}^{d-1}$, access to marginal information allows us to construct a flow with more structure.

Example 4. Consider $\pi_t = \mathcal{N}(\mu_t, \Sigma_t)$ with parameters given by (14) where $\mu_0 = (0, 0)^T$, $\Sigma_0 = I$, $\Sigma_L = \begin{pmatrix} 1 & \rho \\ \rho & 1 \end{pmatrix}$, $y = (14.25, 14.25)^T$ and $\rho = 0.85$. From (14), the independent prior measure simultaneously gets deformed and translated as one moves along the Gaussian curve \mathcal{C}_π . From Figure 2, it is apparent that, on average, particles driven by (16) require less kinetic energy than that of (21)-(22) using the functions g_1 and g_2 specified in Proposition 3. However in the general non-Gaussian case, obtaining the velocity field with minimum kinetic energy requires solving a complex PDE.

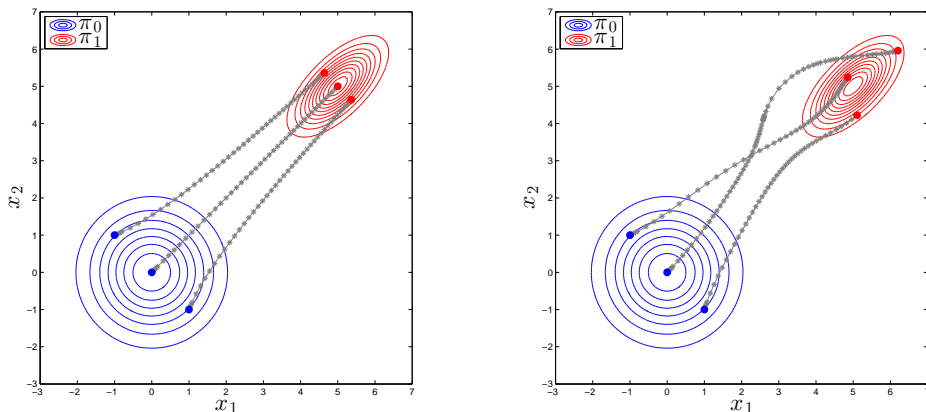


Figure 2: Bivariate Gaussian example. Three particle trajectories driven under different velocity fields but with the same initial conditions in both panels: (*left*) kinetic energy minimizing velocity field (16); (*right*) velocity field in Proposition 2 or equations (21)-(22). The asterisk symbols displayed correspond to steps taken by an adaptive explicit fourth-order Runge-Kutta numerical integrator.

3.4 Gibbs flow approximation

Despite the explicit form of the novel flow transport on \mathbb{R}^d introduced in Proposition 2, this flow still lacks tractability as a numerical implementation would require computing integrals of

dimension up to d . For computational tractability, we propose here to approximate this flow transport with a coupled system of d one-dimensional flow transport problems defined by the full conditional distributions $\{\pi_t(dx_i|x_{-i})\}_{i=1}^d$ of the measure π_t . Each of these one-dimensional flow transport problem only requires the evaluation of one-dimensional integrals in view of Proposition 1. The price to pay for this tractability is that, except when the posterior measure factorizes, the Gibbs flow does not solve the flow transport problem and only approximately tracks the curve of distributions \mathcal{C}_π .

Proposition 4. Consider the Gibbs velocity field $\tilde{f} = (\tilde{f}_1, \dots, \tilde{f}_d)$ defined for $i = 1, 2, \dots, d$ by

$$\tilde{f}_i(x, t) = \frac{-\int_{-\infty}^{x_i} \partial_t \pi_t(u_i|x_{-i}) du_i}{\pi_t(x_i|x_{-i})} = \frac{\lambda'(t) I_t(x_{-i}) (F_t(x_i|x_{-i}) - I_t^{x_i}(x_{-i})/I_t(x_{-i}))}{\pi_t(x_i|x_{-i})}, \quad (24)$$

where $I_t^{x_i}(x_{-i}) = \int_{-\infty}^{x_i} \log L(u_i, x_{-i}) \pi_t(u_i|x_{-i}) du_i$, $I_t(x_{-i}) = \int_{-\infty}^{\infty} \log L(u_i, x_{-i}) \pi_t(u_i|x_{-i}) du_i$ and $F_t(x_i|x_{-i}) = \int_{-\infty}^{x_i} \pi_t(u_i|x_{-i}) du_i$ is the CDF of $\pi_t(dx_i|x_{-i})$. The Gibbs velocity field solves the following system of coupled Liouville equations

$$\partial_{x_i}(\pi_t(x_i|x_{-i}) \tilde{f}_i(x, t)) = -\partial_t \pi_t(x_i|x_{-i}), \quad (25)$$

for $i = 1, 2, \dots, d$, each of which defined on $\mathbb{R} \times (0, 1)$. Additionally, if $\lim_{|x| \rightarrow \infty} L(x) = 0$, then for any initial condition $x_0 \in \mathbb{R}^d$, the ODE associated to the Gibbs flow (24) admits a unique solution on $i(x_0) = [0, 1]$.

Equation (24) is the full conditional analogue of (13), so the interpretations made in Section 3.1 now carry over to each full conditional level. We stress that the Gibbs flow can be computed solely using one-dimensional integrals as the normalizing constant $Z(t)$ cancels in the expression:

$$\tilde{f}_i(x; t) = \lambda'(t) \left\{ F_t(x_i|x_{-i}) \int_{-\infty}^{\infty} \log L(u_i, x_{-i}) \pi_0(u_i, x_{-i}) L(u_i, x_{-i})^{\lambda(t)} du_i - \int_{-\infty}^{x_i} \log L(u_i, x_{-i}) \pi_0(u_i, x_{-i}) L(u_i, x_{-i})^{\lambda(t)} du_i \right\} / \pi_0(x) L(x)^{\lambda(t)}, \quad (26)$$

for $i = 1, 2, \dots, d$ where

$$F_t(x_i|x_{-i}) = \frac{\int_{-\infty}^{x_i} \pi_t(u_i, x_{-i}) du_i}{\int_{-\infty}^{\infty} \pi_t(v_i, x_{-i}) dv_i} = \frac{\int_{-\infty}^{x_i} \pi_0(u_i, x_{-i}) L(u_i, x_{-i})^{\lambda(t)} du_i}{\int_{-\infty}^{\infty} \pi_0(v_i, x_{-i}) L(v_i, x_{-i})^{\lambda(t)} dv_i}.$$

When initialized at $\tilde{\pi}_0 = \pi_0$, under the conditions of Proposition 4, \tilde{f} induces a curve of measures $\mathcal{C}_{\tilde{\pi}} = \{\tilde{\pi}_t\}_{t \in [0, 1]}$ in the sense that $\tilde{f} \in \mathcal{L}(\mathcal{C}_{\tilde{\pi}})$. In the following Proposition, we establish a quantitative bound between $\tilde{\pi}_t$ and π_t as a function of the following time-dependent local error which compares how much this mimics the desired change in mass dictated by (3):

$$\varepsilon_t(x) = \left| \partial_t \pi_t(x) - \nabla \cdot (\pi_t(x) \tilde{f}(x, t)) \right| \quad (27)$$

$$= \left| \partial_t \pi_t(x) - \sum_{i=1}^d \partial_t \pi_t(x_i|x_{-i}) \pi_t(x_{-i}) \right| \quad (28)$$

$$= \lambda'(t) \pi_t(x) \left| \log L(x) - I_t - \sum_{i=1}^d (\log L(x) - I_t(x_{-i})) \right|. \quad (29)$$

In our intuitive derivation of Liouville's equation in Appendix A, we summed over all axes in (49) to obtain the net rate at which probability mass is changing in a given control volume. The sum in (28) reveals that there is no interaction between components of (24), i.e. no information about how much probability mass is changing in a particular direction is shared with the other components, in contrast with the telescopic sum in the proof of Proposition 2. The latter behaviour

is a consequence of breaking down a global problem in d dimensions to d many one-dimensional problems.

For any function $\varphi : \mathbb{R}^d \rightarrow \mathbb{R}$, let $\|\varphi\|_{L^2}^2 = \int_{\mathbb{R}^d} \varphi^2(x) dx < \infty$ and $\|\varphi\|_{\infty} = \sup_{x \in \mathbb{R}^d} |\varphi(x)| < \infty$. We have the following result.

Proposition 5. *Let $\mathcal{C}_{\pi} = \{\pi_t\}_{t \in [0,1]}$ be the curve of measures defined in (2). Assume the conditions of Proposition 4 and denote by $\mathcal{C}_{\tilde{\pi}} = \{\tilde{\pi}_t\}_{t \in [0,1]}$ the curve of measures induced by the Gibbs velocity field (24) when initialized at $\tilde{\pi}_0 = \pi_0$. Then the error involved in the Gibbs flow transport approximation is upper bounded for $t \in (0, 1]$ by*

$$\|\tilde{\pi}_t - \pi_t\|_{L^2}^2 \leq t \int_0^t \|\varepsilon_u\|_{L^2}^2 du \cdot \exp\left(1 + \int_0^t \|\nabla \cdot \tilde{f}(\cdot, u)\|_{\infty} du\right). \quad (30)$$

The bound provided by the above proposition is tight in the sense that it is equal to zero when the posterior measure factorizes. When this is not the case, we observe that the bound deteriorates as expected when t increases. This bound also suggests that the temperature function $\lambda(t)$ should be chosen such that its derivative $\lambda'(t)$ is small at those time instances where the integrated local error $\|\varepsilon_t\|_{L^2}^2$ is large as this would reduce the magnitude of α_t .

To illustrate the nature of the Gibbs flow approximation, we return to Example 4 and observe the error in L^2 -norm at varying degrees of correlation, induced by the parameter ρ , and extremality of the observation y . The left panel of Figure 3 shows that while performance degrades with ρ , as expected, the approximation is able to exploit any local independence structure in the target measures, thus keeping the error reasonably small for small degrees of correlation. The right panel of Figure 3 reveals the inadequacy of the approximation when the overlap between the prior measure and the likelihood decreases, which is to be expected.

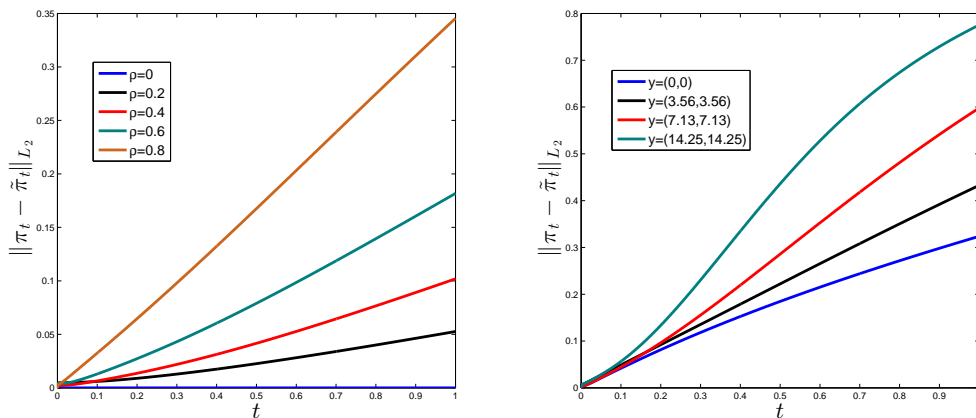


Figure 3: Bivariate Gaussian example. Error in L^2 -norm at varying degrees of correlation ρ (left) and extremality of the observation y (right).

4 Gibbs flow implementation and settings

4.1 Numerical implementation of the Gibbs flow

Consider an ODE with the Gibbs velocity field (24) initialized at $X_0 \sim \pi_0$. A practical implementation of the Gibbs flow involves two source of approximations. Firstly, for most non-trivial problems, the expression of the velocity field will not be analytically tractable so a numerical approximation is necessary. Secondly, as the ODE is typically intractable, the use of a numerical integration scheme is also required. We now detail both approximations.

Recall from (26) that each evaluation of the Gibbs velocity field $\tilde{f}(x, t)$ requires computation of integrals of the form $\int_D \phi(u_i, x_{-i}) du_i$ for some integrand ϕ and domain $D \subseteq \mathbb{R}$. We consider here the class of composite Newton-Cotes quadrature rules

$$\int_D \phi(u_i, x_{-i}) du_i \approx \sum_{i=1}^R \omega_i \phi(u_i, x_{-i}) \quad (31)$$

where $\{\omega_i\}$ are quadrature weights which depend on the degree of the approximation and $\{u_i\}$ are R -many equispaced quadrature points in D [23, p. 34]. We take (31) to be of the closed type, i.e. u_1 and u_R will take the endpoints of D ². In what follows, the latter choice will be convenient when approximating integrals on domains of the type $D = (-\infty, x_i]$ for $x_i < \infty$. The composite quadrature rule (31) is derived by integrating Lagrange interpolation polynomials on subintervals; the degree of which dictates the accuracy of the approximation on each subinterval. We will henceforth denote by $\check{f}(x, t)$ the numerical approximation of the Gibbs velocity field $\tilde{f}(x, t)$.

For ease of presentation, we present here a forward Euler scheme to numerically integrate the ODE at times $t_0 = 0 < t_1 < \dots < t_M = 1$ with the approximate Gibbs velocity field $\check{f}(x, t)$. At time $t = 0$, we initialize a particle by sampling $X_0 \sim \pi_0$. Subsequently, for $n = 1, \dots, M$, we move the particle with location X_{n-1} at time t_{n-1} to location X_n at time $t_n = t_{n-1} + \Delta t_n$ using the iteration

$$X_n = X_{n-1} + \Delta t_n \check{f}(X_{n-1}, t_{n-1}) = \Phi_n(X_{n-1}), \quad (32)$$

which can be rewritten as

$$X_n = \check{T}_{t_n}(X_0) = \Phi_n \circ \Phi_{n-1} \circ \dots \circ \Phi_1(X_0). \quad (33)$$

More intricate higher order methods can also be used to define the mappings Φ_n but since in this context the Jacobian of these maps is needed (see (34) and (36) below), implementation quickly becomes cumbersome. Additional smoothness assumptions would also be needed for those methods to achieve their full potential. For increased stability, implicit methods could also be considered but we prefer embedding a potentially less stable explicit scheme in the control structure afforded by particle weights to solving the nonlinear equations that would otherwise arise.

4.2 Distribution of the Gibbs flow samples

We show here that it is possible to compute the probability distribution $\check{\pi}_{t_n}$ of X_n . This allows us to use the approximate Gibbs flow procedure defined by (32) as a proposal distribution within MCMC, importance sampling or SMC.

Proposition 4 shows that, under mild assumptions, when initialized at $X_0 \sim \pi_0$, the ODE with Gibbs velocity field (24) admits a unique solution $x(t; X_0) = X_t = \tilde{T}_t(X_0)$. The maps \tilde{T}_t are by construction C^1 -diffeomorphisms. Hence the maps \check{T}_{t_n} defined by (32), which are approximations of \tilde{T}_{t_n} , will be injective for sufficiently small step sizes Δt_n and a precise enough quadrature approximation; see [7] for a similar point. Under these conditions, it follows that the probability density $\check{\pi}_{t_n}(x)$ of X_n is given by

$$\check{\pi}_{t_n}(x) = \pi_0(\check{T}_{t_n}^{-1}(x)) |\det \mathcal{J}_{\check{T}_{t_n}}(x)|^{-1} \quad (34)$$

where $|\det \mathcal{J}_{\check{T}_{t_n}}(x)|$ is the absolute value of the determinant of the Jacobian of the map \check{T}_{t_n} and $\check{T}_{t_n}^{-1}$ its inverse, i.e. $\check{T}_{t_n}^{-1} \circ \check{T}_{t_n}(x) = x$. In numerical implementations, monotonicity may be monitored by checking for any sign changes in the determinant of the Jacobian.

It follows from (33) that computing the Jacobian of \check{T}_{t_n} requires the Jacobian of the mappings Φ_k for $k = 1, 2, \dots, n$, which in turn requires the Jacobian of \check{f} . Analytical tractability of the Gibbs velocity field allows us to obtain exact expressions of the Jacobian of \check{f} , see Appendix C. When integrals in \check{f} are replaced by quadrature approximations (31) to obtain \check{f} , it turns out that the

²We can have $u_1 = -\infty$.

Jacobian of \check{f} may be obtained by replacing integrals in the Jacobian of \tilde{f} with approximations based on the same quadrature rule. This result follows straightforwardly for off-diagonal terms of the Jacobian matrix using linearity. For diagonal entries, we have to compute derivatives w.r.t. x_i of approximations of integrals of the form $\int_{-\infty}^{x_i} \phi(u_i, x_{-i}) du_i$, which can be done using the following argument. Denote by $\hat{\phi}$ the underlying Lagrange interpolant giving rise to the quadrature rule (31), then the first fundamental theorem of calculus and the closed property of (31) yields

$$\partial_{x_i} \sum_{i=1}^R \omega_i \phi(u_i, x_{-i}) = \partial_{x_i} \int_{-\infty}^{x_i} \hat{\phi}(u_i, x_{-i}) du_i = \hat{\phi}(x_i, x_{-i}) = \phi(x_i, x_{-i}). \quad (35)$$

Hence independent samples $X_n^{(i)}$, $i = 1, \dots, N$, from $\check{\pi}_{t_n}$ can be weighted consistently w.r.t. to π_{t_n} by using the weights

$$W_n^{(i)} \propto W_{n-1}^{(i)} \frac{\pi_{t_n}(X_n^{(i)})}{\pi_{t_{n-1}}(X_{n-1}^{(i)}) \left| \det \mathcal{J}_{\Phi_n}(X_{n-1}^{(i)}) \right|^{-1}} \quad (36)$$

for $n \geq 1$ with $W_0^{(i)} \propto 1$.

At each time iteration, the computational cost involved is $O(d \times R)$ to perform quadrature and the cost involved in computing the Jacobian of a $d \times d$ matrix. In the most general case, the latter has a computational cost of order $O(d^3)$, although there exists more efficient implementations such as the Strassen algorithm. Moreover, this cost will be significantly lowered in statistical models with conditional independence structure since, by construction, the Gibbs flow exploits such structure to yield sparse Jacobian matrices – see Equation (24). For example, the Jacobian associated to a chain-shaped undirected graphical model is a tridiagonal matrix.

4.3 Combining the Gibbs flow with annealed importance sampling

It is natural to combine the Gibbs flow with AIS [11, 24, 30]. Recall that to perform inference w.r.t. a target $\pi = \pi_1$, AIS also introduces a sequence of intermediate target distributions π_{t_n} where $t_0 = 0 < t_1 < \dots < t_M = 1$. It samples N independent inhomogeneous Markov chains such that $X_0^{(i)} \sim \pi_0$ and $X_n^{(i)} \sim K_n(X_{n-1}^{(i)}, \cdot)$ for $n = 1, \dots, M$ and $i = 1, \dots, N$, where K_n is an MCMC kernel invariant w.r.t. π_{t_n} . An importance sampling argument shows that the samples $X_{n-1}^{(i)}$ can be reweighted consistently w.r.t. to π_{t_n} by using the weights

$$W_n^{(i)} \propto W_{n-1}^{(i)} \frac{\pi_{t_n}(X_{n-1}^{(i)})}{\pi_{t_{n-1}}(X_{n-1}^{(i)})} \quad (37)$$

for $n \geq 1$ with $W_0^{(i)} \propto 1$. If the MCMC kernels mix slowly and/or the discrepancy between successive targets is too high, then the variance of the importance weights can be very high.

To improve the performance of this procedure, references [38, 39] suggested adding deterministic mappings ψ_n which attempt to “push” samples from $\pi_{t_{n-1}}$ closer to π_{t_n} ³. Practically, one initializes by sampling $X_0^{(i)} \sim \pi_0$ and setting $\tilde{X}_0^{(i)} = X_0^{(i)}$ and for $n \geq 1$ iterate by setting $X_n^{(i)} = \psi_n(\tilde{X}_{n-1}^{(i)})$ and sampling $\tilde{X}_n^{(i)} \sim K_n(X_n^{(i)}, \cdot)$. Another importance sampling argument shows that the samples $X_n^{(i)}$ can be weighted consistently w.r.t. to π_{t_n} by using the weights

$$W_n^{(i)} \propto W_{n-1}^{(i)} \frac{\pi_{t_n}(X_n^{(i)})}{\pi_{t_{n-1}}(\tilde{X}_{n-1}^{(i)}) \left| \det \mathcal{J}_{\psi_n}(\tilde{X}_{n-1}^{(i)}) \right|^{-1}} \quad (38)$$

³As mentioned in the introduction, these authors realized that it is possible to theoretically map samples from $\pi_{t_{n-1}}$ to π_{t_n} using an ODE whose drift solves the Liouville PDE [38] but they did not propose a generic methodology to approximate such a drift.

with $W_0^{(i)} \propto 1$. In Section 5, we will use this procedure with the mapping ψ_n given by Φ_n defined in (32).

To assess the accuracy of the resulting importance sampling approximation of π_{t_n} , it is common to monitor the effective sample size (ESS) introduced in [25] which is given by

$$\text{ESS} = \left(\sum_{i=1}^N \left(W_n^{(i)} \right)^2 \right)^{-1}.$$

This criterion takes values between 1 and N . Whenever ESS is small, say $\text{ESS} < N/2$, it is beneficial to perform resampling and assign uniform weights to the resampled particles. The resulting algorithm can be interpreted as a special instance of SMC sampler [15]⁴.

Lastly, we revisit Example 4. Figure 4 illustrates the difference in terminal particle locations when running solely Gibbs flow, AIS and combining Gibbs flow with AIS. We observe that the combination of the diffusive behavior of the MCMC kernels used within AIS steps and the deterministic mappings of the Gibbs flow steps provide particles whose terminal positions overlap much better with the support of the target than using solely Gibbs flow or AIS.

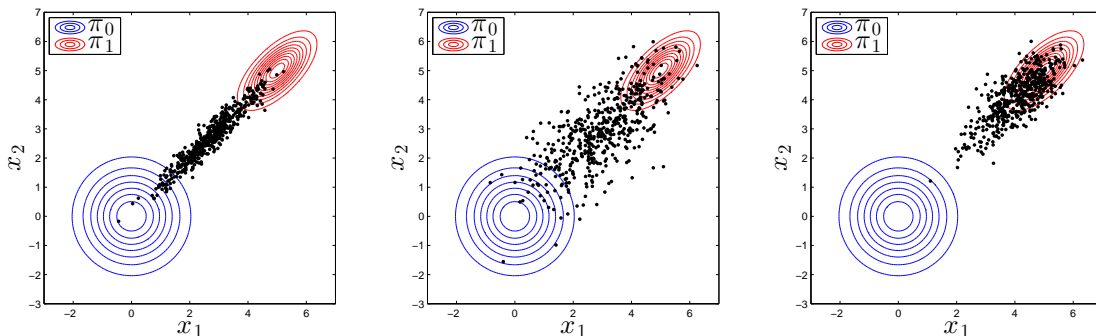


Figure 4: Bivariate Gaussian example. Terminal particle positions of $N = 500$ prior samples whose evolution were prescribed by: (left) Gibbs flow iteration in (32); (middle) AIS with random walk Metropolis-Hastings (RWMH) kernels; (right) combining (32) with the corresponding RWMH kernel used in AIS.

4.4 Selecting the temperature function

The temperature function λ in (2), which controls the rate at which we want to introduce the likelihood, has a significant impact on the performance of the aforementioned methodology. In the context of path sampling and SMC samplers, various schemes have been proposed to select this function; see e.g. [21, 42].

For our purposes, recall that the upper bound in Proposition 5 dictates that λ should be chosen such that its derivative is small whenever the time-dependent integrated local errors is large. The latter is typically substantial whenever there are large changes between intermediate distributions. Noting that large changes along \mathcal{C}_π necessarily imply large changes in the corresponding full conditionals, the time steps $\{\Lambda_n\}$ taken by an adaptive scheme to numerically integrate the Gibbs ODE may be used to guide the choice of a suitable temperature function λ , since large variations in (24) will require smaller step sizes to keep estimates of numerical integration error below a prespecified tolerance.

⁴In the SMC sampler terminology, the backward kernel associated to the deterministic mapping ψ_n is given by the optimal backward kernel specified in equation (25) of [15] and the backward kernel associated to the MCMC kernel K_n is its associated reversal kernel.

We demonstrate this on the curve of measures (39) arising from a Bayesian mixture modelling application detailed further in Section 5. Observe from Figure 5 that with a linear temperature function, large changes along the curve \mathcal{C}_π occur at very early times. We advocate here that λ should be prescribed such that the time steps $\{\Lambda_n\}$ taken by an adaptive numerical integrator is as close as possible to being equispaced on $[0, 1]$ – up to some variability between different initial conditions. Figure 6 shows that this can be achieved in this case by setting $\lambda(t) = t^6$.

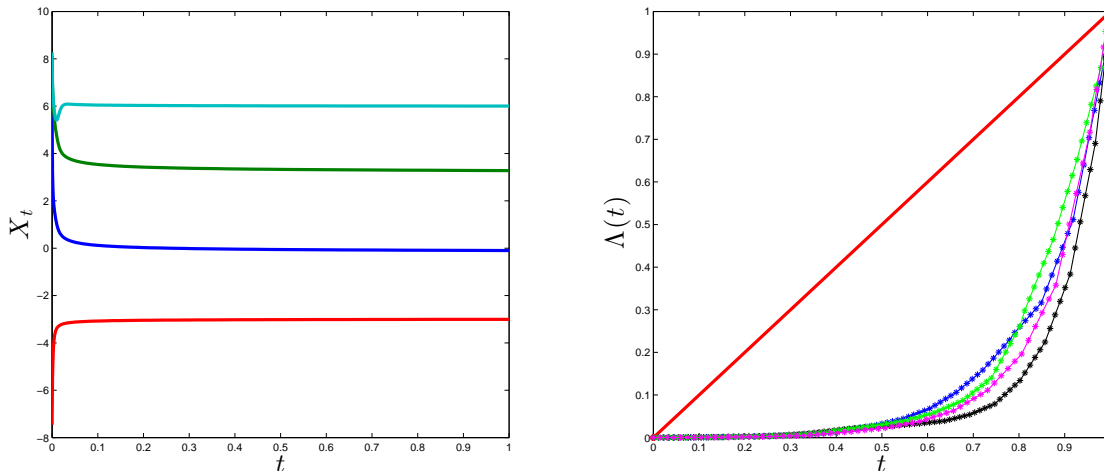


Figure 5: Mixture modelling example with $\lambda(t) = t$. (Left) Trajectory of a particle under Gibbs flow with different colors representing each dimension. (Right) Colored lines correspond to the time steps taken by an adaptive numerical integrator for four different prior samples evolving under the Gibbs flow to be compared against the red identity line.

5 Applications

5.1 Bayesian mixture modelling

5.1.1 Model description

We now demonstrate performance of the Gibbs flow on a Bayesian Gaussian mixture model where the posterior distribution of mixture means is inferred. This is a canonical example of distributions with multiple well-separated models.

Consider independent observations $\{y_j\}_{j=1}^m$ from a univariate Gaussian mixture model with d components, i.e. each observation is distributed according to the density $\frac{1}{d} \sum_{i=1}^d \phi(y_j; x_i, \sigma_i^2)$, where $\phi(\cdot; \mu, \varsigma)$ denotes a univariate Gaussian density with mean μ and variance ς . We follow [26] by setting $d = 4$, $\sigma_i = \sigma = 0.55$ for $i = 1, 2, \dots, d$ and perform inference only on the mean parameters $x \in \mathbb{R}^4$. We generate the data $\{y_j\}_{j=1}^m$ using $m = 100$ simulations from the model with parameter value of $x^* = (-3, 0, 3, 6)^T$ and stratification between components. Ascribing a uniform prior on the d -dimensional hypercube $[-10, 10]^d$, i.e. $\pi_0 = \mathcal{U}([-10, 10]^d)$, the curve of measures \mathcal{C}_π is simply

$$\pi_t(x) = \frac{\mathbb{I}_{[-10, 10]^d}(x) L(x)^{\lambda(t)}}{20^d Z(t)} \quad (39)$$

for $t \in [0, 1]$, where

$$L(x) = \frac{1}{d^m} \prod_{j=1}^m \sum_{i=1}^d \phi(y_j; x_i, \sigma^2). \quad (40)$$

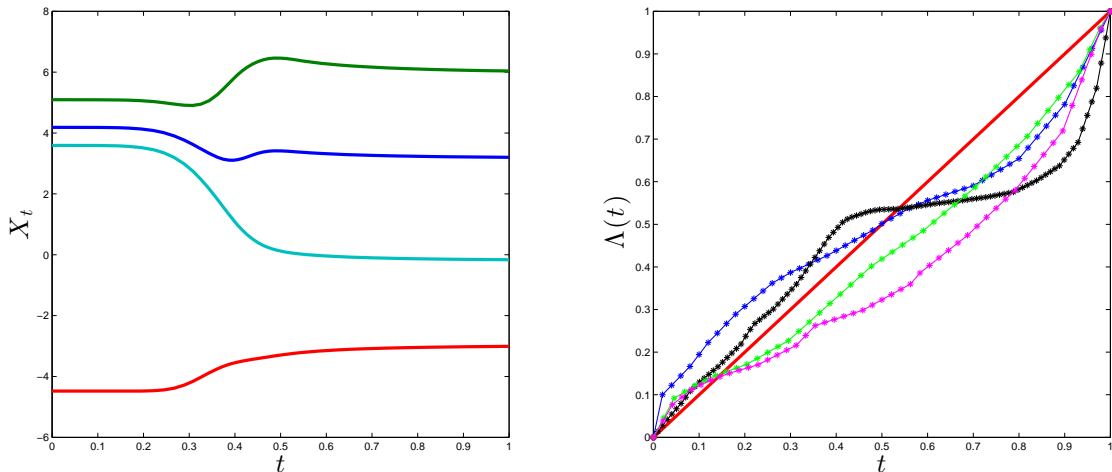


Figure 6: Mixture modelling example with $\lambda(t) = t^6$. (Left) Trajectory of a particle under Gibbs flow with different colors representing each dimension. (Right) Colored lines correspond to the time steps taken by an adaptive numerical integrator for four different prior samples evolving under the Gibbs flow to be compared against the red identity line.

It follows from exchangeability of the prior and non-identifiability of mixture components that the posterior measure is invariant under “label permutation”. As such, π_1 admits $d! = 24$ well-separated modes centered approximately around permutations of x^* .

5.1.2 Gibbs flow settings and performance

The Gibbs flow approximation. Firstly, we investigate the quality of the Gibbs flow approximation, before employing any importance sampling correction. We do so by comparing the time evolution of $N = 1000$ prior samples under the Gibbs flow with the output of a standard SMC sampler (described in [26]) as the reference truth in Figure 7. The performance of the approximation for this challenging problem is striking; particles are able to reach all 24 modes in \mathbb{R}^4 . This is corroborated in Figure 8 which plots the marginal posteriors on \mathbb{R}^2 for all pairs (note that each of these admit 12 well-separated modes) and in Figure 9 which displays the proportion of particles in each of the 24 modes when the initial particle locations were taken as a latin hypercube sample of size $N = 1000$ (to reduce the variance from prior sampling). We note that the similarity in the proportions observed at each mode demonstrates the “global” nature of the Gibbs flow approximation.

Comparison of algorithmic performance. We now compare the Gibbs flow (Section 4.2), AIS with Metropolis-adjusted Langevin algorithm (MALA) moves and a method combining the Gibbs flow with AIS using random walk MH (RWMH) moves (Section 4.3). Following the discussion in Section 4.4, we set $\lambda(t) = t^6$. The choice of numerical integration scheme is the forward Euler scheme with step size selected so that monotonicity of the mappings defined in (33) is ensured. Using the left panel of Figure 6, we prescribe a piecewise linear time discretization to focus computational efforts at times with more particle movement. At each time iteration, we allow the AIS sampler and the Gibbs-AIS sampler to make 10 MCMC moves which are tuned to achieve average acceptance probabilities in the range of (0.15, 0.4). All one-dimensional integrals involved in evaluations of the Gibbs velocity field and its Jacobian are computed using a composite Simpsons rule with 50 quadrature points.

Algorithmic performance is measured in terms of ESS. To yield a fair comparison, we set the number of time steps taken by each algorithm so as to match computational cost. The results

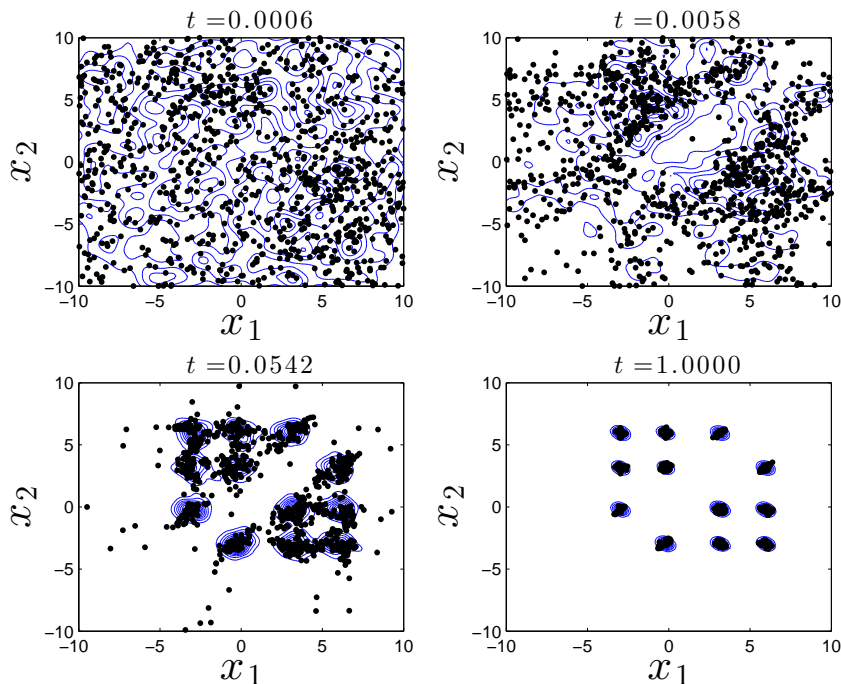


Figure 7: Time evolution of $N = 1000$ prior samples under the Gibbs flow (*black dots*). For each time instance, the superimposed blue contours represent the target measure obtained as a kernel density estimate from the output of a standard SMC sampler.

displayed in Figure 10 show that the Gibbs-AIS sampler outperforms the other algorithms. The poor performance of the sampler based solely on Gibbs flow can be seen in Figure 7 and 8; as the distribution of samples under the Gibbs flow has thinner tails than the target distribution, it is a poor importance distribution. The latter is not a difficulty when one combines Gibbs flow with AIS owing to the diffusivity introduced in the MCMC moves.

5.2 Sampling truncated multivariate Gaussians for high-dimensional probit models

5.2.1 Model and Gibbs flow description

So far we have restricted our attention to problems where we build the curve of measures C_π by tempering a likelihood function L . We show here that these assumptions can be relaxed by adapting the Gibbs flow approximation to sample from truncated multivariate Gaussian distributions and illustrate in Section 5.2.3 how this procedure can be included in a MCMC algorithm to perform inference for a Bayesian multivariate probit model.

Let $\pi_0 = \mathcal{N}(\mu, \Sigma)$ be a multivariate Gaussian on \mathbb{R}^d and call the truncated measure π . Assume that the truncation happens component-wise, i.e. $\text{supp}(\pi) = \prod_{i=1}^d (a_i, b_i)$ where $a_i, b_i \in \bar{\mathbb{R}}$ and $a_i < b_i$ for all $i = 1, 2, \dots, d$. If the truncation is extreme, it is natural to form a set of bridging distributions by performing the truncation gradually. In other words, we build a curve of measures C_π via

$$\pi_t(x) = \frac{\pi_0(x) \prod_{i=1}^d \mathbb{I}_{(\alpha_i(t), \beta_i(t))}(x_i)}{Z(t)}, \quad (41)$$

where $\alpha_i(t) < \beta_i(t)$ for all $t \in [0, 1]$, $\alpha_i : [0, 1] \rightarrow \bar{\mathbb{R}}$ is non-decreasing with boundary conditions $\alpha_i(0) = -\infty$, $\alpha_i(1) = a_i$, $\beta_i : [0, 1] \rightarrow \bar{\mathbb{R}}$ non-increasing with boundary conditions $\beta_i(0) = \infty$,

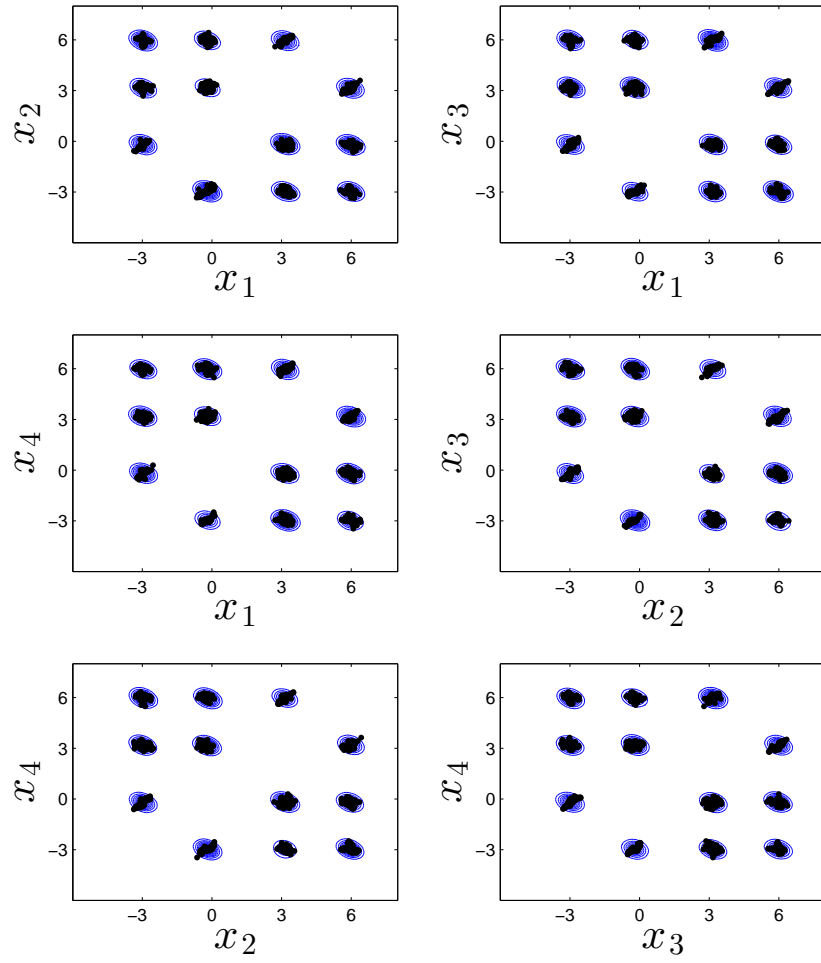


Figure 8: All pairs of marginal posterior measures on \mathbb{R}^2 .

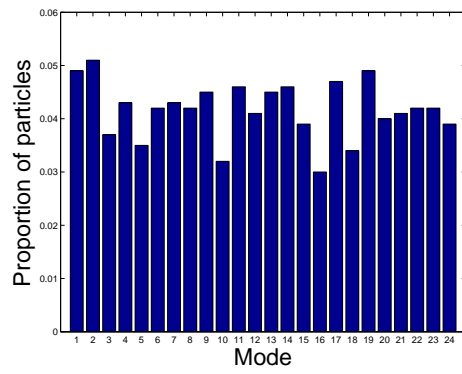


Figure 9: Proportion of particles in each of the 24 modes in \mathbb{R}^4 .

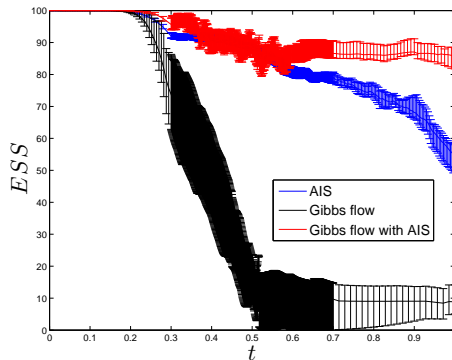


Figure 10: Time evolution of ESS. Lines and error bars indicate median and interquartile range, respectively, of 20 repetitions.

$\beta_i(1) = b_i$, and $Z(t) = \pi_0(\prod_{i=1}^d (\alpha_i(t), \beta_i(t)))$. From these assumptions, it is clear that C_π connects π_0 to $\pi_1 = \pi$. In contrast to having a temperature function, α_i and β_i now control the rate of truncation. It may be shown that

$$\partial_t \pi_t(x_i | x_{-i}) = (\alpha'_i(t) \pi_t(\alpha_i(t) | x_{-i}) - \beta'_i(t) \pi_t(\beta_i(t) | x_{-i})) \pi_t(x_i | x_{-i}), \quad (42)$$

for $x \in \text{supp}(\pi_t) = \prod_{i=1}^d (\alpha_i(t), \beta_i(t))$. In the same manner as in Proposition 4, we can solve the system of Liouville equations (25) with

$$\tilde{f}_i(x, t) = \frac{\alpha'_i(t) \pi_0(\alpha_i(t), x_{-i}) \int_{x_i}^{\beta_i(t)} \pi_0(u_i, x_{-i}) du_i + \beta'_i(t) \pi_0(\beta_i(t), x_{-i}) \int_{\alpha_i(t)}^{x_i} \pi_0(u_i, x_{-i}) du_i}{\pi_0(x) \int_{\alpha_i(t)}^{\beta_i(t)} \pi_0(u_i, x_{-i}) du_i}. \quad (43)$$

The expressions for the Jacobian of \tilde{f} are given in Appendix D. As in Section 4.2, the Jacobian of \tilde{f} under quadrature approximation can simply be computed by replacing the integrals in the Jacobian of \tilde{f} by their quadrature approximations.

5.2.2 Gibbs flow settings and performance

To address a similar problem, [28] proposed a method based on SMC sampler [15] and reported computational gains in comparison to the one-at-a-time Gibbs sampler when the degree of correlation in the multivariate Gaussian is significant. We adopt the simulation study in [28] and compare an SMC sampler based solely on Gibbs flow, AIS with RWMH moves and an SMC sampler which combines Gibbs flow with RWMH moves. Before proceeding, we note that MALA moves are not employed within AIS; the use of gradient information of π is not appropriate in this context as the gradient might point to directions of zero probability mass. On the contrary, flow transport provides a principled way to drift particles towards the right regions of the state space.

The effect of correlation. Consider $d = 4$, a mean vector of $\mu = (-\xi, -\xi, \xi, \xi)^T$ for $\xi > 0$, which keeps two components in the truncation region of $\text{supp}(\pi) = [0, \infty)^d$. For starters, we set $\xi = 1$. The off-diagonal elements of Σ are set to a value such that all pairwise correlations are equal to $\rho \in [0, 1]$. As before, the numerical integration scheme used is the forward Euler scheme with step size selected so that monotonicity of the mappings defined in (33) is ensured. Using insight from preliminary simulations of the Gibbs flow, we perform the truncation with $\alpha_i(t) = -1/t + 1$ for all $i = 1, 2, \dots, d$ and select a piecewise linear time discretization to focus computational efforts at times with more particle movement. At each time iteration, we allow AIS and the Gibbs flow-AIS method to make 50 RWMH moves. The covariance of the Gaussian random walk is set as $\sigma \Sigma$ with $\sigma > 0$ tuned to achieve average acceptance probabilities in the range of (0.15, 0.4). All

one-dimensional integrals involved in evaluations of the Gibbs velocity field and its Jacobian are computed using a composite Simpsons rule with 40 quadrature points.

We perform the same ESS comparison as before by not resampling and setting the number of time steps taken by each algorithm to match computational cost. The left panel of Figure 11 shows how the ESS of each sampler vary with the correlation parameter ρ . The results are striking and interesting; the performance of samplers based on Gibbs flow degrades with ρ whilst the AIS sampler which uses only RWMH moves improves with ρ . This behaviour clearly illustrates the Gibbs flow’s ability to exploit any local independence structure in π_0 .

The effect of truncation extremality. Again for dimensionality of $d = 4$, we now fix the correlation parameter at $\rho = 0.5$ and vary the location parameter ξ in the middle panel of Figure 11. All other algorithmic settings are the same as before. The results show that as the truncation becomes extreme, the Gibbs flow can mitigate particle degeneracy by moving particles towards the right regions of the state space.

The effect of dimension. We now set correlation at $\rho = 0.5$, truncation at $\xi = 1$ and vary dimension d . Algorithmic settings are the same as before except that we now allow the number of RWMH moves taken at each time iteration to increase linearly with dimension. The results, summarized in the right panel of Figure 11, show that while the performance of algorithms degrade with dimension, which is to be expected, combining flow transport with MCMC has the potential to allow SMC samplers to remain competitive in high dimensions.

Normalizing constant estimation. Lastly, we compare the performance of these algorithms to estimate the normalizing constant $Z(1) = \pi_0([0, \infty)^d)$ as the correlation parameter ρ , the location parameter ξ and dimension d varies one at a time. Algorithmic settings are the same as above with the exception of applying systematic resampling whenever ESS falls below half of the number of particles used. As performance measure, in Figure 12 we plot the ratio of the estimated standard deviation of the AIS (with resampling steps) estimator to the estimated standard deviation of the Gibbs flow and Gibbs flow-AIS with resampling estimators. The results are similar to those obtained in the ESS comparisons and show that the Gibbs flow with AIS estimator provides significantly lower variance estimators of the unknown normalizing constant.

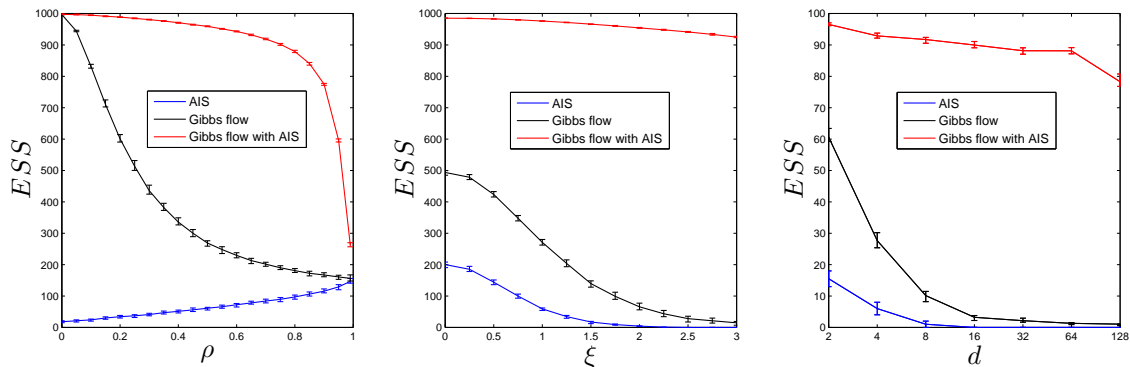


Figure 11: Comparison of ESS between algorithms as the correlation parameter ρ (*left*), the location parameter ξ (*middle*) and dimension d (*right*) varies one at a time. Lines and error bars indicate median and interquartile range, respectively, of 100 repetitions.

5.2.3 Bayesian multivariate probit model

We now apply the above procedure to the Bayesian multivariate probit model discussed in [37]. Denote by $Y \in \{0, 1\}^{n \times J}$ the J -dimensional binary responses on n subjects, $X \in \mathbb{R}^{n \times p}$ the design

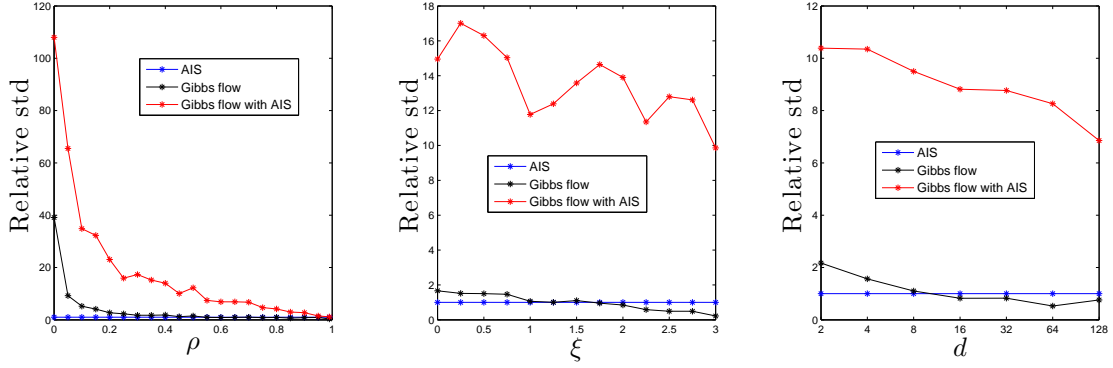


Figure 12: Estimated relative standard deviation (with AIS as benchmark) based on 100 repetitions as the correlation parameter ρ (left), the location parameter ξ (middle) and dimension d (right) varies one at a time.

matrix, $\beta \in \mathbb{R}^{p \times J}$ the regression coefficients and $R \in \mathbb{R}^{J \times J}$ a correlation matrix. For each subject $Y_i \in \{0, 1\}^J$ ($i = 1, 2, \dots, n$), the multivariate probit model specifies that

$$\mathbb{P}(Y_i = y_i | X, \beta, R) = \int_{\mathcal{I}_i} \phi_J(z_i; (X\beta)_i, R) dz_i, \quad (44)$$

where $(X\beta)_i$ is the i^{th} row of $X\beta$ and $\mathcal{I}_i = \mathcal{I}_{i1} \times \mathcal{I}_{i2} \times \dots \times \mathcal{I}_{iJ}$ with $\mathcal{I}_{ij} = [0, \infty)$ if $y_{ij} = 1$ and $(-\infty, 0)$ otherwise. Note that the restriction of R to correlation matrices in (44) ensures likelihood identifiability [8]. Equation (44) also prompts characterization of the model using Gaussian latent variables $Z \in \mathbb{R}^{n \times J}$ with $Y_{ij} = \mathbb{I}_{(Z_{ij} \geq 0)}$.

We assign a prior distribution to β, R and the graph structure G of the inverse correlation matrix R^{-1} . Interest here is sampling from the resulting posterior

$$\pi(G, R, \beta, Z | y) \propto \pi(G) \pi(R | G) \pi(\beta | R) \pi(Z | \beta, R) \prod_{i=1}^n \mathbb{I}_{(Z_i \in \mathcal{I}_i)}. \quad (45)$$

Our choice of prior is similar to [37] which showed that it is possible to sample from the posterior using a Gibbs update for Z and β , a simple MH random walk on the space of graphs G and a parameter expansion data augmentation step for R . For the latent Gaussian variables, the full conditional density factorizes as

$$\pi(Z | \beta, R, y, G) \propto \prod_{i=1}^n \phi_J(Z_i | (X\beta)_i, R) \mathbb{I}_{(Z_i \in \mathcal{I}_i)}. \quad (46)$$

The sampling scheme used in [37] samples each Z_i by updating its components one-at-a-time using a Gibbs sampler which slows down convergence of the resulting algorithm. Instead, here we employ the above Gibbs-AIS sampler for truncated Gaussians, but implemented as a conditional SMC update to ensure validity within the resulting Gibbs sampler.

5.2.4 Six cities dataset

We now apply the above methodology to analyze a well-known dataset from the Six Cities longitudinal study on the health effects of air pollution.

Description. The dataset concerned contains repeated binary measurements of $n = 537$ children's wheezing status from Steubenville, Ohio. Interest here is on modelling the probabilistic relation over time of the wheezing status of a child as a function of their age and their mother's

smoking habit during the first year of the study. Notationally, the binary response y_{ij} indicates if child $i = 1, 2, \dots, n$ was wheezing in the $j = 1, 2, 3, 4$ year of the study (corresponding to when the subject was of age 7, 8, 9, 10 respectively).

The nature of the data suggest that using a multivariate probit model to account for the structure of association between components of the multivariate binary response is appropriate. Also, table 1 supports having mothers' smoking habits as a covariate.

We note that similar analysis have been conducted on this particular dataset with differing inference procedures; see [8, 37, 28].

Mother's smoking status	7	8	9	10
Smoker	32 (17.0%)	40 (21.3%)	36 (19.1%)	27 (14.4%)
Non-smoker	55 (15.8%)	51 (14.6%)	49 (14.0%)	36 (10.0%)
Total	87 (16.2%)	91 (16.9%)	85 (15.8%)	63 (11.7%)

Table 1: Breakdown of wheezing cases by age group and initial smoking status of mothers. Percentages are with respect to each age group.

Algorithmic settings. Settings within the conditional Gibbs-AIS sampler used to update Z involved 10 particles with multinomial resampling triggered when the ESS falls before 5; a linear time discretization with 50 steps and 20 RWMH moves with covariance of the Gaussian random walk tuned to achieve suitable acceptance probabilities. We run $N = 22,000$ iterations of the Gibbs sampler described earlier (burn-in of 2000 samples), with estimation of the graph structure. We obtained similar results to [37] for both posterior means and graph structure (not displayed).

Results. Table 2 gives the posterior mean and standard deviation of parameters in the model.

	Posterior mean	Posterior standard deviation
β_{11}	-0.9207	0.091
β_{12}	0.030	0.154
β_{21}	-0.9845	0.092
β_{21}	0.222	0.151
β_{31}	-1.012	0.096
β_{32}	0.180	0.156
β_{41}	-1.179	0.100
β_{42}	0.170	0.165
R_{12}	0.496	0.069
R_{13}	0.423	0.073
R_{14}	0.483	0.073
R_{23}	0.588	0.058
R_{24}	0.470	0.075
R_{34}	0.549	0.066

Table 2: Posterior mean and standard deviation of parameters in the multivariate probit model.

Acknowledgements

Arnaud Doucet's research is partially supported by the Engineering and Physical Sciences Research Council (grant EP/K000276/1, EP/K009850/1).

References

- [1] L. Ambrosio. Transport equation and Cauchy problem for BV vector fields. *Inventiones mathematicae*, 158(2):227–260, 2004.
- [2] L. Ambrosio, N. Gigli, and G. Savaré. *Gradient Flows in Metric Spaces And in the Space of Probability Measures*. Lectures in Mathematics ETH Zurich. Birkhauser, 2005.
- [3] C. Andrieu, A. Doucet and R. Holenstein. Particle Markov chain Monte Carlo methods (with Discussion). *Journal of the Royal Statistical Society: Series B*, 72(3):269–342, 2010.
- [4] A.R. Barron and X. Luo. Adaptive annealing. In *Proceedings of the Allerton Conference on Communications, Computation and Control*, 665–673, 2007.
- [5] K. Bergemann and S. Reich. An ensemble Kalman-Bucy filter for continuous data assimilation. *Meteorologische Zeitschrift*, 21(3):213–219, 2012.
- [6] O. Bokanowski and B. Grébert. Deformations of density functions in molecular quantum chemistry. *Journal of Mathematical Physics*, 37(4):1553–1573, 1996.
- [7] P. Bunch and S.J. Godsill. Approximations of the optimal importance density using Gaussian particle flow importance sampling. *Journal of the American Statistical Society*, to appear. Technical report arXiv:1406.3183, 2014.
- [8] S. Chib and E. Greenberg. Analysis of multivariate probit models. *Biometrika*, 85(2):347–361, 1998.
- [9] A. Chkifaa, A. Cohen and C. Schwab. Breaking the curse of dimensionality in sparse polynomial approximation of parametric PDEs. *Journal de Mathématiques Pures et Appliquées*, 103(2):400–428, 2015.
- [10] D. Crisan and J. Xiong. Approximate McKean–Vlasov representations for a class of SPDEs. *Stochastics*, 82(1):53–68, 2010.
- [11] G.E. Crooks. Nonequilibrium measurements of free energy differences for microscopically reversible Markovian systems. *Journal of Statistical Physics*, 90(5-6):1471–1487, 1998.
- [12] B. Dacorogna and J. Moser. On a partial differential equation involving the Jacobian determinant. *Annales de l’Institut Henri Poincaré C (Analyse non linéaire)*, 7:1–26, 1990.
- [13] W. Dahmen, R. Devore, L. Grasedyck and E. Süli. Tensor-sparsity of solutions to high-dimensional elliptic partial differential equations. *Foundations of Computational Mathematics*, 1-62, 2014.
- [14] F. Daum and J. Huang. Particle flow and Monge-Kantorovich transport. In *Proceedings Conference on Information Fusion*, 135–142, 2012.
- [15] P. Del Moral, A. Doucet, and A. Jasra. Sequential Monte Carlo samplers. *Journal of the Royal Statistical Society: Series B*, 68(3):411–436, 2006.
- [16] P. Del Moral. *Feynman-Kac Formulae*. New York: Springer, 2004.
- [17] R. J. DiPerna and P. L. Lions. Ordinary differential equations, transport theory and Sobolev spaces. *Inventiones Mathematicae*, 98(3):511–547, 1989.
- [18] A. Doucet, J.F.G. De Freitas, and N.J. Gordon (eds.). *Sequential Monte Carlo Methods in Practice*. New York: Springer-Verlag, 2001.
- [19] T.A. El Moselhy and Y.M. Marzouk. Bayesian inference with optimal maps. *Journal of Computational Physics*, 231(23):7815–7850, 2012.
- [20] C.W. Gardiner. *Handbook of Stochastic Methods for Physics, Chemistry and the Natural Sciences*. 2nd edition, Springer, 2002.

- [21] A. Gelman and X.-L. Meng. Simulating normalizing constants: From importance sampling to bridge sampling to path sampling. *Statistical Science*, 13(2):163–185, 1998.
- [22] R.E. Greene and K. Shiohama. Diffeomorphisms and volume-preserving embeddings of non-compact manifolds. *Transactions of the American Mathematical Society*, 255:403–403, 1979.
- [23] A. Iserles. *A First Course in the Numerical Analysis of Differential Equations*. Cambridge University Press, 2009.
- [24] C. Jarzynski. Nonequilibrium equality for free energy differences. *Physical Review Letters*, 78(14), 2690, 1997.
- [25] A. Kong, J.S. Liu and W.H. Wong. Sequential imputations and Bayesian missing data problems. *Journal of the American Statistical Association*, 89(425):278–288, 1994.
- [26] A. Lee, C. Yau, M.B. Giles, A. Doucet and C.C. Holmes. On the utility of graphics cards to perform massively parallel simulation of advanced Monte Carlo methods. *Journal of Computational and Graphical Statistics*, 19(4):769–789, 2010.
- [27] X-L. Meng and S. Schilling. Warp bridge sampling. *Journal of Computational and Graphical Statistics*, 11(3):552–586, 2002.
- [28] G. Moffa and J. Kuipers. Sequential Monte Carlo EM for multivariate probit models. *Computational Statistics and Data Analysis*, 72:252–272, 2014.
- [29] J. Moser. On the volume elements on a manifold. *Transactions of the American Mathematical Society*, 120(2):286–294, 1965.
- [30] R.M. Neal. Annealed importance sampling. *Statistics and Computing*, 11(2):125–139, 2001.
- [31] E. Novak and H. Wozniakowski. Approximation of infinitely differentiable multivariate functions is intractable. *J. Complexity*, 25:398–404, 2009.
- [32] S. Reich. A dynamical systems framework for intermittent data assimilation. *BIT Numerical Analysis*, 51:235–249, 2011.
- [33] S. Reich. A Gaussian-mixture ensemble transform filter. *Quarterly Journal of the Royal Meteorological Society*, 138(662):222–233, 2012.
- [34] S. Reich and C.J. Cotter. *Probabilistic Forecasting and Bayesian Data Assimilation*. Cambridge University Press, 2015.
- [35] A.M. Stuart and A.R. Humphries. *Dynamical Systems and Numerical Analysis*. Cambridge University Press, 1998.
- [36] Y. Tao, P.G. Mehta, and S.P. Meyn. Feedback particle filter. *IEEE Transactions on Automatic Control*, 58(10):2465–2480, 2013.
- [37] A. Talhouk, A. Doucet and K. Murphy. Efficient Bayesian inference for multivariate probit models with sparse inverse correlation matrices. *Journal of Computational and Graphical Statistics*, 21(3):739–757, 2012.
- [38] S. Vaikuntanathan and C. Jarzynski. Escorted free energy simulations: Improving convergence by reducing dissipation. *Physical Review Letters*, 100(19), 190601, 2008.
- [39] S. Vaikuntanathan and C. Jarzynski. Escorted free energy simulations. *Journal of Chemical Physics*, 134(5), 054107, 2011.
- [40] C. Villani. *Optimal Transport: Old and New*. Springer Berlin Heidelberg, 2008.
- [41] W. Walter. *Ordinary Differential Equations*. Springer, 1998.
- [42] Y. Zhou, A.M. Johansen and J.A.D. Aston. Towards automatic model comparison: an adaptive sequential Monte Carlo approach. *Journal of Computational and Graphical Statistics*, to appear. Technical report arXiv:1303.3123.

A Proofs of Section 2

Informal derivation of Liouville's equation. □

Consider a d -dimensional hyper-rectangle $\Delta V(x)$ defined formally as the Cartesian product of intervals $(x_i, x_i + \Delta_i), i = 1, 2, \dots, d$, to be thought of as an infinitesimal control volume at the point $x \in \mathbb{R}^d$ – see Figure A.

If we perceive particles as constituents of a fluid representing probability mass, then the fluid flow driven by a velocity field f will cause the probability mass in $\Delta V(x)$ to change. Along each axis i , for sufficiently small $\Delta = (\Delta_1, \Delta_2, \dots, \Delta_d)$, this change is given by the difference between the rate at which mass flows into $\Delta V(x)$

$$\pi_t(x) f_i(x, t) \prod_{j \neq i} \Delta_j + o(|\Delta|_\infty^d) \quad (47)$$

and the rate at which mass flows out of $\Delta V(x)$

$$\pi_t(x + \Delta_i e_i) f_i(x + \Delta_i e_i, t) \prod_{j \neq i} \Delta_j + o(|\Delta|_\infty^d), \quad (48)$$

where $\{e_i\}_{i=1}^d$ denote the canonical basis vectors for \mathbb{R}^d . In fluid dynamics terminology, the terms in (47) and (48) are simply the density multiplied by the volume metric flow rate in and out of the control volume.

Now summing over all axes yields the net rate at which probability mass is changing in $\Delta V(x)$:

$$\sum_{i=1}^d \left(\pi_t(x) f_i(x, t) \prod_{j \neq i} \Delta_j - \pi_t(x + \Delta_i e_i) f_i(x + \Delta_i e_i, t) \prod_{j \neq i} \Delta_j \right) + o(|\Delta|_\infty^d). \quad (49)$$

For probability mass to be conserved, (49) has to be equal to

$$\partial_t \pi_t(x) \prod_{i=1}^d \Delta_i + o(|\Delta|_\infty^d). \quad (50)$$

Equating (49) and (50) and dividing by the volume $\prod_{i=1}^d \Delta_i$ gives

$$\sum_{i=1}^d \frac{\pi_t(x) f_i(x, t) - \pi_t(x + \Delta_i e_i) f_i(x + \Delta_i e_i, t)}{\Delta_i} = \partial_t \pi_t(x) + o(1). \quad (51)$$

Finally, taking the limit of $\Delta \rightarrow 0$ yields the Liouville PDE:

$$-\sum_{i=1}^d \partial_{x_i} (\pi_t(x) f_i(x, t)) = \partial_t \pi_t(x). \quad (52)$$

Proof of Lemma 1. Using the dominated convergence theorem with dominating function $\pi_0(x) L(x)^{\lambda(t)} \leq \pi_0(x) \sup_{t \in [0, 1]} L(x)^{\lambda(t)} \leq \pi_0(x) (1 + L(x))$ shows that $Z(t)$ is continuous on $[0, 1]$. Together with continuity of $\lambda(t)$, it then follows that $t \mapsto \pi_t(x) \in C^0([0, 1], \mathbb{R}^+)$ for each $x \in \mathbb{R}^d$. Hence for any bounded function $\varphi \in C^0(\mathbb{R}^d, \mathbb{R})$ and any sequence $(t_n)_{n \geq 1} \subset [0, 1]$ such that $t_n \rightarrow t_*$, we have $\varphi(x) \pi_{t_n}(x) \rightarrow \varphi(x) \pi_{t_*}(x)$ pointwise. Note that

$$|\varphi(x) \pi_{t_n}(x)| \leq \sup_{u \in \mathbb{R}^d} |\varphi(u)| \frac{\pi_0(x) \sup_{t \in [0, 1]} L(x)^{\lambda(t)}}{\inf_{t \in [0, 1]} Z(t)}. \quad (53)$$

Since $Z(t)$ is continuous on $[0, 1]$, the infimum in (53) is attained and is strictly positive under positivity assumptions made on $\pi_0(x)$ and $L(x)$. Hence the upper bound in (53) is integrable and by the dominated convergence theorem, we have $\lim_{n \rightarrow \infty} \int_{\mathbb{R}^d} \varphi(x) \pi_{t_n}(dx) = \int_{\mathbb{R}^d} \varphi(x) \pi_{t_*}(dx)$, as desired. □

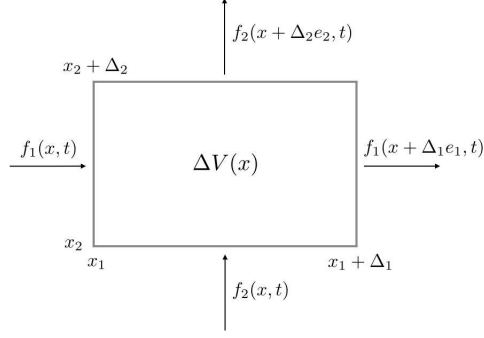


Figure 13: Illustrating the conservation of mass argument in \mathbb{R}^2 .

B Proofs of Section 3

Proof of Proposition 1. Using continuity of π_0, L and positivity of L , an application of the first fundamental theorem of calculus shows that $f \in \mathcal{L}(\mathcal{C}_\pi)$. The assumptions on π_0 and L imply $f \in C^1(\mathbb{R} \times [0, 1], \mathbb{R})$; hence for any compact set $K \subset \mathbb{R}$, its derivative is bounded on $K \times [0, 1]$ and local Lipschitzness A1 follows. The integrability condition A2 follows from the prescribed tail behaviour that there exists an $\epsilon > 0$ such that $x \mapsto |f(x, t)| \pi_t(x) = O(|x|^{-1-\epsilon})$ as $|x| \rightarrow \infty$ for all $t \in [0, 1]$. Hence $f \in \mathcal{L}(\mathcal{C}_\pi) \cap \mathcal{E}(\mathcal{C}_\pi)$ and appealing to theorem 1 shows that (11) solves the flow transport problem. To see that (11) is indeed the minimal kinetic energy solution, we note that the optimality condition in [32, 33] requires existence of a function $\varphi : \mathbb{R} \times [0, 1] \rightarrow \mathbb{R}$ such that $f(x, t) = \nabla \varphi(x, t)$ and $\partial_t \pi_t = -\nabla \cdot (\pi_t \nabla \varphi)$. The former is trivially satisfied as a consequence of working on \mathbb{R} since we may set $\varphi(x, t) = \int_c^x f(u, t) du < \infty$ for any $c < x$ and the latter follows since $f \in \mathcal{L}(\mathcal{C}_\pi)$. \square

Proof of Proposition 2. The arguments are similar to those used in Proposition 1. By straightforward verification $f \in \mathcal{L}(\mathcal{C}_\pi)$:

$$\begin{aligned}
\nabla \cdot (\pi_t f) &= \sum_{i=1}^d \partial_{x_i} (\pi_t(x) f_i(x, t)) \\
&= - \sum_{i=1}^{d-1} \partial_{x_i} \left(\prod_{j=1}^{i-1} g'_j(x_j, t) \int_{\mathbb{R}^{i-1}} \int_{-\infty}^{x_i} \partial_t \pi_t(u_{1:i-1}, u_i, x_{i+1:d}) du_{1:i-1} du_i \right. \\
&\quad \left. - \prod_{j=1}^{i-1} g'_j(x_j, t) g_i(x_i, t) \int_{\mathbb{R}^i} \partial_t \pi_t(u_{1:i}, x_{i+1:d}) du_{1:i} \right) \\
&\quad - \partial_{x_d} \left(\prod_{j=1}^{d-1} g'_j(x_j, t) \int_{\mathbb{R}^{d-1}} \int_{-\infty}^{x_d} \partial_t \pi_t(u_{1:d-1}, u_d) du_{1:d-1} du_d \right) \\
&= - \sum_{i=1}^{d-1} \left(\prod_{j=1}^{i-1} g'_j(x_j, t) \int_{\mathbb{R}^{i-1}} \partial_t \pi_t(u_{1:i-1}, x_i, x_{i+1:d}) du_{1:i-1} \right. \\
&\quad \left. - \prod_{j=1}^i g'_j(x_j, t) \int_{\mathbb{R}^i} \partial_t \pi_t(u_{1:i}, x_{i+1:d}) du_{1:i} \right) \\
&\quad - \prod_{j=1}^{d-1} g'_j(x_j, t) \int_{\mathbb{R}^{d-1}} \partial_t \pi_t(u_{1:d-1}, x_d) du_{1:d-1} \\
&= -\partial_t \pi_t.
\end{aligned}$$

The penultimate line applies the first fundamental theorem of calculus and the final equality comes from the telescopic sum. The assumptions on π_0, L and $\{g_i\}_{i=1}^{d-1}$ imply $f \in C^1(\mathbb{R}^d \times [0, 1], \mathbb{R}^d)$; hence local Lipschitzness A1 follows. The integrability condition A2 follows from the prescribed tail behaviour that there exists an $\epsilon > 0$ such that $x \mapsto |f(x, t)| \pi_t(x) = O(|x|^{-1-\epsilon})$ as $|x| \rightarrow \infty$ for all $t \in [0, 1]$. Hence $f \in \mathcal{L}(\mathcal{C}_\pi) \cap \mathcal{E}(\mathcal{C}_\pi)$ and appealing to Theorem 1 completes the proof. \square

Proof of Proposition 3. Note that by the above choice $g'_i(x_i, t) = \pi_t(x_i)$. From (21), for $i = 1, 2, \dots, d-1$

$$\begin{aligned}
f_i(x, t) &= \lambda'(t) \left(\prod_{j=1}^{i-1} \pi_t(x_j) \int_{-\infty}^{x_i} \int_{\mathbb{R}^{i-1}} \left(I_t - \sum_{l=1}^i \log L_l(u_l) - \sum_{k=i+1}^d \log L_k(x_k) \right) \right. \\
&\quad \times \prod_{j=1}^i \pi_t(u_j) \prod_{k=i+1}^d \pi_t(x_k) du_{1:i-1} du_i \\
&\quad - \prod_{j=1}^{i-1} \pi_t(x_j) \int_{-\infty}^{x_i} \pi_t(u_i) du \int_{\mathbb{R}^i} \left(I_t - \sum_{l=1}^i \log L_l(u_l) - \sum_{k=i+1}^d \log L_k(x_k) \right) \\
&\quad \times \prod_{j=1}^i \pi_t(u_j) \prod_{k=i+1}^d \pi_t(x_k) du_{1:i} \Big) / \prod_{l=1}^d \pi_t(x_l), \\
&= \lambda'(t) \left(\int_{-\infty}^{x_i} \pi_t(u_i) du_i \left(I_t - \sum_{l=1}^{i-1} I_t^{(l)} - \sum_{k=i+1}^d \log L_k(x_k) \right) - \int_{-\infty}^{x_i} \log L_i(u_i) \pi_t(u_i) du_i \right. \\
&\quad \left. - \int_{-\infty}^{x_i} \pi_t(u_i) du_i \left(I_t - \sum_{l=1}^i I_t^{(l)} - \sum_{k=i+1}^d \log L_k(x_k) \right) \right) / \pi_t(x_i) \\
&= \lambda'(t) \left(\int_{-\infty}^{x_i} (I_t^{(i)} - \log L_i(u_i)) \pi_t(u_i) du_i \right) / \pi_t(x_i), \tag{54}
\end{aligned}$$

and from (22)

$$\begin{aligned}
f_d(x, t) &= \lambda'(t) \left(\prod_{j=1}^{d-1} \pi_t(x_j) \int_{-\infty}^{x_d} \int_{\mathbb{R}^{d-1}} \sum_{l=1}^d (I_t^{(l)} - \log L_l(u_l)) \prod_{k=1}^d \pi_t(u_k) du_{1:d-1} du_d \right) / \prod_{l=1}^d \pi_t(x_l), \\
&= \lambda'(t) \left(\int_{-\infty}^{x_d} \pi_t(u_d) du_d \left(\sum_{l=1}^d I_t^{(l)} - \sum_{l=1}^{d-1} I_t^{(l)} \right) - \int_{-\infty}^{x_d} \log L_d(u_d) \pi_t(u_d) du_d \right) / \pi_t(x_d) \\
&= \lambda'(t) \left(\int_{-\infty}^{x_d} (I_t^{(d)} - \log L_d(u_d)) \pi_t(u_d) du_d \right) / \pi_t(x_d). \tag{55}
\end{aligned}$$

\square

Proof of Proposition 4. Routine application of the first fundamental theorem of calculus and using continuity of π_0, L shows that the coupled system of ODEs corresponding to (24) solves (25). The assumptions on π_0 and L imply $\tilde{f} \in C^1(\mathbb{R}^d \times [0, 1], \mathbb{R}^d)$; hence for any compact set $K \subset \mathbb{R}^d$, its derivative is bounded on $K \times [0, 1]$ and local Lipschitzness follows.

Recall that since \tilde{f} is locally Lipschitz, we need to demonstrate that the solution is bounded whenever it exists to complete the proof. Boundedness will be obtained by showing that $V(x) = |x|^2$ is a Lyapunov function. It may be shown that

$$\partial_t \pi_t(x_i | x_{-i}) = \lambda'(t) (\log L(x) - I_t(x_{-i})) \pi_t(x_i | x_{-i}), \tag{56}$$

where $I_t(x_{-i}) = \int_{-\infty}^{\infty} \log L(u_i, x_{-i}) \pi_t(u_i | x_{-i}) du_i$. By assumption $|\log L(x)| \rightarrow \infty$ as $|x| \rightarrow \infty$, so for each $x_{-i} \in \mathbb{R}^{d-1}$, there exists $R_i > 0$ such that $\log L(x) < I_t(x_{-i})$ for $|x_i| > R_i$. This implies

that $x_i \mapsto -x_i \int_{-\infty}^{x_i} \partial_t \pi_t(u_i | x_{-i}) du_i = x_i \int_{x_i}^{\infty} \partial_t \pi_t(u_i | x_{-i}) du_i < 0$. Therefore we may choose a sufficiently large $R > 0$ such that

$$\frac{d}{dt} V(x) = 2 \langle x, \tilde{f}(x, t) \rangle < 0, \quad (57)$$

for $x \in \mathbb{R}^d \setminus B(0, R)$. It follows that $|x(t; x_0)| < \max\{R, |x_0|\}$ and hence $i(x_0) = [0, 1]$. \square

Proof of Proposition 5. Choose an $f \in \mathcal{L}(\mathcal{C}_\pi) \cap \mathcal{E}(\mathcal{C}_\pi)$. Note that the time evolution of the measures $\{\tilde{\pi}_t\}_{t \in [0, 1]}$ induced by \tilde{f} is governed by another Liouville equation:

$$-\nabla \cdot (\tilde{\pi}_t \tilde{f}) = \partial_t \tilde{\pi}_t. \quad (58)$$

Define $\Delta : \mathbb{R}^d \times [0, 1] \rightarrow \mathbb{R}$ as the difference $\Delta_t = \pi_t - \tilde{\pi}_t$. By taking the difference between

$$-\nabla \cdot (\pi_t f) = \partial_t \pi_t \quad (59)$$

and (58) and introducing a cross term, we obtain

$$-\nabla \cdot (\pi_t(f - \tilde{f}) + \Delta_t \tilde{f}) = \partial_t \Delta_t. \quad (60)$$

Multiplying throughout by Δ_t and applying chain rule yields

$$-(\nabla \cdot \tilde{f}) \Delta_t^2 - \frac{1}{2} \langle \tilde{f}, \nabla \Delta_t^2 \rangle - \nabla \cdot (\pi_t(f - \tilde{f})) \Delta_t = \frac{1}{2} \partial_t \Delta_t^2. \quad (61)$$

We then integrate by parts and note that the boundary term vanishes:

$$-\int_{\mathbb{R}^d} (\nabla \cdot \tilde{f}) \Delta_t^2 - 2 \int_{\mathbb{R}^d} \nabla \cdot (\pi_t(f - \tilde{f})) \Delta_t = \partial_t \|\Delta_t\|_{L^2}^2. \quad (62)$$

Now for each $t \in [0, 1]$, using Hölder's and Young's inequalities, yields

$$\partial_t \|\Delta_t\|_{L^2}^2 \leq \left| \int_{\mathbb{R}^d} (\nabla \cdot \tilde{f}) \Delta_t^2 \right| + 2 \left| \int_{\mathbb{R}^d} \nabla \cdot (\pi_t(f - \tilde{f})) \Delta_t \right| \quad (63)$$

$$\leq \|\nabla \cdot \tilde{f}(\cdot, t)\|_\infty \|\Delta_t\|_{L^2}^2 + \|\Delta_t\|_{L^2}^2 / \delta + \delta \|\varepsilon_t\|_{L^2}^2 \quad (64)$$

for any $\delta > 0$. Integrating both sides of (63) on $[0, t]$, we have

$$\|\Delta_t\|_{L^2}^2 \leq \delta \int_0^t \|\varepsilon_u\|_{L^2}^2 du + \int_0^t \left(\|\nabla \cdot \tilde{f}(\cdot, u)\|_\infty + 1/\delta \right) \|\Delta_u\|_{L^2}^2 du, \quad (65)$$

to which Gronwall's lemma on the time interval $[0, t]$ combined with the fact that $t \mapsto \delta \int_0^t \|\varepsilon_u\|_{L^2}^2 du$ is non-decreasing yields

$$\|\Delta_t\|_{L^2}^2 \leq \delta \int_0^t \|\varepsilon_u\|_{L^2}^2 du \cdot \exp\left(t/\delta + \int_0^t \|\nabla \cdot \tilde{f}(\cdot, u)\|_\infty du\right). \quad (66)$$

Now by minimizing this upper bound w.r.t δ , we obtain (30). \square

C Jacobian matrix of Gibbs flow

Consider the form of \tilde{f} given in (26). For notational ease, write $\tilde{f}_i(x, t) = N_i(x, t)/\gamma_t(x)$ where N_i is the numerator and $\gamma_t(x, t) = \pi_0(x)L(x)^{\lambda(t)}$ is the unnormalized density. Now for $(x, t) \in \mathbb{R}^d \times [0, 1]$, consider the (i, k) -th element of the Jacobian matrix $\mathcal{J}_{\tilde{f}}(x, t)$:

$$\begin{aligned} \partial_{x_k} \tilde{f}_i(x, t) &= \tilde{f}_i(x, t) \partial_{x_k} \log \tilde{f}_i(x, t) \\ &= \tilde{f}_i(x, t) (\partial_{x_k} \log N_i(x, t) - \partial_{x_k} \log \gamma_t(x)) \\ &= \frac{\partial_{x_k} N_i(x, t)}{\gamma_t(x)} - \tilde{f}_i(x, t) \partial_{x_k} \log \gamma_t(x). \end{aligned}$$

Note first that

$$\partial_{x_k} \log \gamma_t(x) = \partial_{x_k} \log \pi_0(x) + \lambda(t) \partial_{x_k} \log L(x).$$

The tricky term to compute is

$$\begin{aligned} \frac{\partial_{x_k} N_i(x, t)}{\gamma_t(x)} &= \lambda'(t) \left\{ \partial_{x_k} F_t(x_i | x_{-i}) \int_{-\infty}^{\infty} \log L(u_i, x_{-i}) \gamma_t(u_i, x_{-i}) du_i \right. \\ &\quad + F_t(x_i | x_{-i}) \partial_{x_k} \left(\int_{-\infty}^{\infty} \log L(u_i, x_{-i}) \gamma_t(u_i, x_{-i}) du_i \right) \\ &\quad \left. - \partial_{x_k} \left(\int_{-\infty}^{x_i} \log L(u_i, x_{-i}) \gamma_t(u_i, x_{-i}) du_i \right) \right\} / \gamma_t(x). \end{aligned}$$

For the diagonal entries, i.e. $k = i$, this is

$$\frac{\partial_{x_i} N_i(x, t)}{\gamma_t(x)} = \lambda'(t) \left\{ \frac{\int_{-\infty}^{\infty} \log L(u_i, x_{-i}) \gamma_t(u_i, x_{-i}) du_i}{\int_{-\infty}^{\infty} \gamma_t(u_i, x_{-i}) du_i} - \log L(x) \right\}.$$

The terms needed in off-diagonal entries are

$$\partial_{x_k} F_t(x_i | x_{-i}) = \int_{-\infty}^{x_i} \partial_{x_k} \log \pi_t(u_i, x_{-i}) \pi_t(u_i | x_{-i}) du_i - F_t(x_i | x_{-i}) \int_{-\infty}^{\infty} \partial_{x_k} \log \pi_t(u_i, x_{-i}) \pi_t(u_i | x_{-i}) du_i,$$

and

$$\begin{aligned} \partial_{x_k} \left(\int \log L(u_i, x_{-i}) \gamma_t(u_i, x_{-i}) du_i \right) &= \int \partial_{x_k} \log L(u_i, x_{-i}) \gamma_t(u_i, x_{-i}) du_i \\ &\quad + \int \log L(u_i, x_{-i}) \gamma_t(u_i, x_{-i}) \partial_{x_k} \log \gamma_t(u_i, x_{-i}) du_i \end{aligned}$$

with appropriate limits.

D Jacobian matrix of Gibbs flow for truncated Gaussians

For notational ease, write (43) as $\tilde{f}_i(x, t) = \frac{N_i(x, t)}{\pi_0(x) \int_{\alpha_i(t)}^{\beta_i(t)} \pi_0(u_i, x_{-i}) du_i}$, where N_i denotes the numerator. Now for $(x, t) \in \text{supp}(\pi_t) \times [0, 1]$, consider the (i, k) -th element of the Jacobian matrix $\mathcal{J}_{\tilde{f}}(x, t)$:

$$\begin{aligned} \partial_{x_k} \tilde{f}_i(x, t) &= \tilde{f}_i(x, t) \partial_{x_k} \log \tilde{f}_i(x, t) \\ &= \tilde{f}_i(x, t) \left(\partial_{x_k} \log N_i(x, t) - \partial_{x_k} \log \pi_0(x) - \partial_{x_k} \log \left(\int_{\alpha_i(t)}^{\beta_i(t)} \pi_0(u_i, x_{-i}) du_i \right) \right) \\ &= \frac{\partial_{x_k} N_i(x, t)}{\pi_0(x) \int_{\alpha_i(t)}^{\beta_i(t)} \pi_0(u_i, x_{-i}) du_i} - \tilde{f}_i(x, t) \left(\partial_{x_k} \log \pi_0(x) + \partial_{x_k} \log \left(\int_{\alpha_i(t)}^{\beta_i(t)} \pi_0(u_i, x_{-i}) du_i \right) \right). \end{aligned}$$

The tricky term to compute is

$$\begin{aligned} \partial_{x_k} N_i(x, t) &= \alpha_i'(t) \pi_0(\alpha_i(t), x_{-i}) \partial_{x_k} \log \pi_0(\alpha_i(t), x_{-i}) \int_{x_i}^{\beta_i(t)} \pi_0(u_i, x_{-i}) du_i \\ &\quad + \alpha_i'(t) \pi_0(\alpha_i(t), x_{-i}) \int_{x_i}^{\beta_i(t)} \partial_{x_k} \log \pi_0(u_i, x_{-i}) \pi_0(u_i, x_{-i}) du_i \\ &\quad + \beta_i'(t) \pi_0(\beta_i(t), x_{-i}) \partial_{x_k} \log \pi_0(\beta_i(t), x_{-i}) \int_{\alpha_i(t)}^{x_i} \pi_0(u_i, x_{-i}) du_i \\ &\quad + \beta_i'(t) \pi_0(\beta_i(t), x_{-i}) \int_{\alpha_i(t)}^{x_i} \partial_{x_k} \log \pi_0(u_i, x_{-i}) \pi_0(u_i, x_{-i}) du_i. \end{aligned}$$

Hence the diagonal entries, i.e. $k = i$, are

$$\partial_{x_i} \tilde{f}_i(x, t) = \frac{\beta'_i(t) \pi_0(\beta_i(t), x_{-i}) - \alpha'_i(t) \pi_0(\alpha_i(t), x_{-i})}{\int_{\alpha_i(t)}^{\beta_i(t)} \pi_0(u_i, x_{-i}) du_i} - \tilde{f}_i(x, t) \partial_{x_i} \log \pi_0(x).$$

The term needed in off-diagonal entries are

$$\partial_{x_k} \log \left(\int_{\alpha_i(t)}^{\beta_i(t)} \pi_0(u_i, x_{-i}) du_i \right) = \frac{\int_{\alpha_i(t)}^{\beta_i(t)} \partial_{x_k} \log \pi_0(u_i, x_{-i}) \pi_0(u_i, x_{-i}) du_i}{\int_{\alpha_i(t)}^{\beta_i(t)} \pi_0(u_i, x_{-i}) du_i}. \quad (67)$$

Lastly, note that for multivariate Gaussian $\pi_0 = \mathcal{N}(\mu, \Sigma)$, we have

$$\nabla \log \pi_0(x) = \Sigma^{-1}(\mu - x). \quad (68)$$